VOLTAGE SAG AND SWELL MITIGATION USING GREY WOLF OPTIMIZER (GWO) FOR A SINGLE-PHASE GRID-CONNECTED PHOTOVOLTAIC SYSTEM

JEFF COLLVEN ANAK CLAISDELL LORREN

B. ENG (HONS.) ELECTRICAL ENGINEERING (POWER SYSTEM)

UNIVERSITI MALAYSIA PAHANG

UNIVERSITI MALAYSIA PAHANG

DECLARATION OF THESIS AND COPYRIGHT

Author's Full Name   : Jeff Collven Anak Claisdell Lorren

Date of Birth   : 4th August 1997

Title   : Voltage sag and swell mitigation using Grey Wolf Optimizer (GWO) for a single-phase grid-connected photovoltaic system

Academic Session   : 2021/2022

I declare that this thesis is classified as:

☐   CONFIDENTIAL   (Contains confidential information under the Official Secret Act 1997)*

☐   RESTRICTED   (Contains restricted information as specified by the organization where research was done)*

☑   OPEN ACCESS   I agree that my thesis to be published as online open access (Full Text)

I acknowledge that Universiti Malaysia Pahang reserves the following rights:

1. The Thesis is the Property of Universiti Malaysia Pahang
2. The Library of Universiti Malaysia Pahang has the right to make copies of the thesis for the purpose of research only.
3. The Library has the right to make copies of the thesis for academic exchange.

Certified by:

_____
(Student's Signature)

_____
(Supervisor's Signature)

970804-13-6227_____
New IC/Passport Number
Date: 27th June 2022

Norazila Binti Jaalam_____
Name of Supervisor
Date:27th June 2022

NOTE : * If the thesis is CONFIDENTIAL or RESTRICTED, please attach a thesis declaration letter.

SUPERVISOR'S DECLARATION

I hereby declare that I have checked this thesis and in my opinion, this thesis is adequate in terms of scope and quality for the award of the degree of Electrical Engineering (Power System).

_____
(Supervisor's Signature)

Full Name   : Norazila Binti Jaalam

Position   : Senior Lecturer

Date   : 27th June 2022

_____
(Co-supervisor's Signature)

Full Name   :

Position   :

Date   :

STUDENT'S DECLARATION

I hereby declare that the work in this thesis is based on my original work except for quotations and citations which have been duly acknowledged. I also declare that it has not been previously or concurrently submitted for any other degree at Universiti Malaysia Pahang or any other institutions.

_____

(Student's Signature)

Full Name   : Jeff Collven Anak Claisdell Lorren

ID Number   : EC18043

Date   : 27th June 2022

VOLTAGE SAG AND SWELL MITIGATION USING GREY WOLF OPTIMIZER (GWO) FOR A SINGLE-PHASE GRID-CONNECTED PHOTOVOLTAIC SYSTEM

JEFF COLLVEN ANAK CLAISDELL LORREN

Thesis submitted in fulfillment of the requirements
for the award of the
Bachelor of Electrical Engineering with Honours

College of Engineering

UNIVERSITI MALAYSIA PAHANG

JUNE 2022

ACKNOWLEDGEMENTS

ABSTRAK

Cabaran kualiti kuasa yang paling menonjol dalam mempengaruhi rangkaian pengedaran ialan voltan "sag" dan "swell" terutamanya dalam sektor industri dimana kerugian merupakan perkara utama dapat dielakkan. Oleh itu, isu kualiti kuasa mesti diselesaikan secepat mungkin bagi menjimatkan wang dan tenaga elektrik. Kos tenaga elektrik yang lebih rendah dan harga kuasa reaktif memberikan faedah secara langsung kepada pelanggan. Penjimatan tidak langsung dibuat dengan menghalang situasi seperti kerosakan peralatan dan penuaan pramatang, kehilangan produktiviti, dan kehilangan data dan kerja. Objektif utama penyelidikan ini adalah untuk mereka bentuk strategi kawalan mudah dengan menggunakan Proportional Integral - Grey Wolf Optimizer (PI-GWO) untuk mengurangkan voltan "sag" dan "swell" semasa keadaan grid lemah. Penyelidikan membentangkan teknik pengoptimuman yang baru dibangunkan dan cekap dipanggil GWO buat pertama kali untuk menyelesaikan gangguan kualiti kuasa dalam sistem bersambung grid satu fasa. Pengoptimuman serigala kelabu (GWO) ialah pendekatan pengoptimuman meta-heuristik baharu yang berdasarkan pengaruh hierarki kepimpinan semulajadi serigala dan mekanisme memburu. Reka bentuk yang dicadang memerlukan tatasusunan Photovoltaic (PV) untuk disambungkan dengan sistem bersambung grid satu fasa. Pertama, fotovoltaik 5MW dibina untuk menghasilkan bekalan kuasa sebelum disambungkan ke grid elektrik. Kemudian, pada bahagian grid eletrik, konfigurasi voltan "sag" dan "swell" digunakan untuk menunjukkan kerosakan satu fasa yang biasanya berlaku dalam grid elektrik - voltan "sag" dan "swell". PI-GWO diperkenalkan ke dalam sistem untuk mengurangkan isu kualiti kuasa dan menganalisis keberkesanannya di bawah peratusan voltan "sag" dan "swell" yang berbeza. Didapati bahawa 10% dan 20% voltan "sag" dan "swell" dapat dikurangkan dengan menggunakan pengawal PI-GWO untuk sistem fotovoltaik yang disambungkan grid fasa tunggal.

iii

ABSTRACT

The most prominent power quality challenges affecting distribution networks are voltage sag and swell, especially in sectors where losses can be significant. The reason that the power quality issue must be resolved as soon as possible is that high power quality may save money and energy. Lower energy costs and reactive power pricing provide direct benefits to customers. Indirect savings are realized by avoiding situations such as equipment damage and premature aging, productivity loss, and data and work loss. The main objective of this research is to design a simple control strategy by using the Proportional Integral-Grey Wolf Optimizer (PI-GWO) to mitigate voltage sag and swell during weak grid conditions. The research presents a newly developed and efficient optimization technique called GWO for the first time to solve power quality disturbances in single-phase grid-connected systems. Grey wolf optimization (GWO) is a new meta-heuristic optimization approach based on the influence of wolves' natural leadership hierarchy and hunting mechanism. The proposed design required the photovoltaic (PV) array to be connected to a single-phase grid-connected system. First, a 5MW photovoltaic power supply is developed before being connected to the grid. Then, at the grid section, voltage sag and swell configurations are applied to show the single-phase faults that normally occur in the grid – voltage sag and swell. PI-GWO is introduced into the system to mitigate the power quality issue and analyze its effectiveness under different percentages of voltage sag and swell. It is found that the 10% and 20% of voltage sag and swell could be mitigate by using PI-GWO controller for a single-phase grid-connected photovoltaic system.

TABLE OF CONTENT

LIST OF TABLES

LIST OF FIGURES

LIST OF SYMBOLS

°C	Degree Celsius
A	Ampere
MW	Mega Watts
V	Voltage
W	Watts

LIST OF ABBREVIATIONS

ACO	Ant Colony Optimization
CO_2	Carbon Dioxide
DG	Distributed generation
DPFC	Distributed Power Flow Controller
DSSC	Dye-sensitized solar cell
DVR	Dynamic Voltage Restorer
FACTS	Flexible Alternative Current Transmission System
GA	Genetic Algorithm
GWO	Grey Wolf Optimizer
IDVR	Interline Dynamic Voltage Restorer
I-V	Current-voltage
Ki	Integral Gain
Kp	Proportional Gain
LFMFO	Levy Flight – Moth Flame Optimization
MFO	Moth Flame Optimization
PI	Proportional-integral
PI-GWO	Proportional Integral – Grey Wolf Optimizer
PLC	Programmable Logic Controller
PQ	Power quality
PSO	Particle Swarm Optimizer
PV	Photovoltaic
P-V	Power-voltage
PWM	Pulse Width Modulation
RES	Renewable Energy Source
RMS	Root-Mean-Square
SG	Smart grid
STATCOM	Static Synchronous Compensator
UPFC	Unified Power Flow Controller

CHAPTER 1

INTRODUCTION

1.1   Project background

The world's energy needs are met by fossil fuels. However, in order to minimise carbon dioxide (CO_2) emissions and adhere to the Kyoto Protocol, the Malaysian government is turning to non-renewable energy resources (Shah Alam et al., 2013). The Kyoto Protocol sets the United Nations Framework Convention on Climate Change into action by committing developed and developing nations to restrict and reduce greenhouse gas (GHG) emissions in line with agreed-upon individual objectives. The Convention merely requires these nations to establish mitigation plans and actions and to report on a regular basis (Iwata & Okada, 2014).

Solar energy is the most cost-effective and pollution-free of all the renewable energy sources (RESs). As a result, photovoltaic (PV) systems are appropriate for meeting growing energy needs while avoiding pollution in the atmosphere (Rajput et al., 2018). This attribute has led to global government initiatives focused on promoting the deployment of grid-connected PV systems that are connected to utility power networks and can export electricity to them (Naidoo & Pillay, 2007). PV systems are typically deployed in a highly dispersed mode in the lowest voltage parts of the grid (down to residential end-use voltages), posing unique challenges for power system engineers trying to figure out how high PV penetration levels in industrial parks or "solar subdivisions" might affect system operations. Because of widespread concern about the environment and the use of non-renewable energy sources, the use of alternative energy sources is rapidly increasing. This fact drives the development of new technologies and research to find solutions that will allow new systems to be connected to the grid in a safe and reliable manner. Small PV system installations might benefit from single-phase PV grid-connected systems (Arafa et al., 2017). In this case, a well-validated computer model

1

would be useful. One of the primary sources of harmonic distortion of current and voltage waveforms is the penetration of PV systems in either transmission or distribution networks. As a result, this is becoming a major issue, particularly at both transmission and distribution levels (El-Sayed et al., 2017). The issue refers to the power quality disturbance such as voltage sag and swell at weak grid conditions which due to single-phase faults or varying irradiance on PV system (Premkumar et al., 2019).

According to IEE Standard 1159-1995, the term "swell" is defined as an increase in root-mean-square (RMS) voltage at the power frequency for a duration of 0.5 cycles to 1 minute, with typical magnitudes of between 1.1 and 1.8 p.u. (Association, 1995). Voltage sags are described as a drop in RMS voltage at the power frequency across time periods ranging from 0.5 to 1 minute. The duration of a voltage sag is the interval between when the rms voltage drops below 0.9 p.u. of nominal voltage and when it climbs over 0.9 p.u. of nominal voltage. As a result, sags of short duration may create issues with some sensitive equipment (Naidoo & Pillay, 2007). Switching processes associated with a transient supply disconnection, the flow of in-rush currents associated with the beginning of motor loads, or the flow of fault currents can all induce voltage sag. These events might be caused by the customer's system or the public supply network. Momentary sags can be caused by lightning strikes. (Mehranfar et al., 2011)

1.2   Problem statement
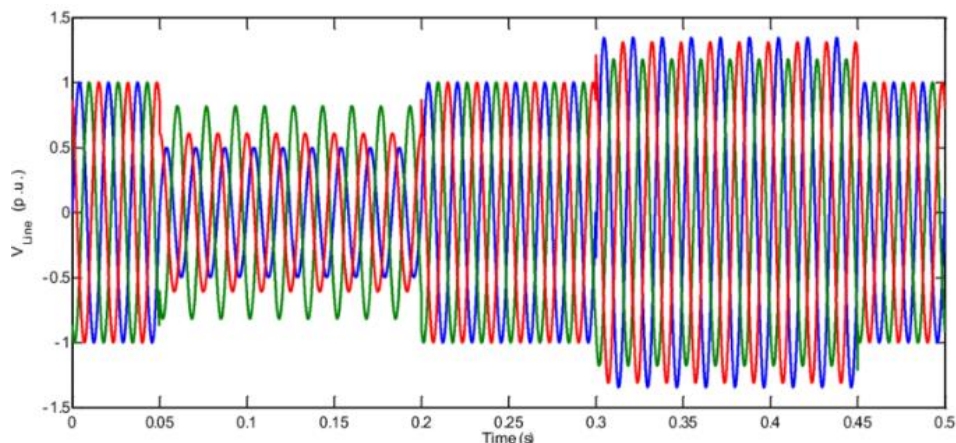
Figure 1.1   Voltage sag and swell scope

Figure 1.1 illustrates the scope of voltage sag and swell which caused the power quality faults. The increased usage of solid state switching devices, nonlinear and power electronically switched loads, unbalanced power systems, lighting controls, computers, and data processing equipment, as well as industrial plant rectifiers and inverters, has resulted in power supply quality challenges and problems (Pakharia & Gupta, 2012). Quasistatic harmonic dynamic voltage distortions, inrush, pulse-type current phenomena with excessive harmonics, and severe distortion are all caused by these electronic-type loads. A change in the electric service voltage or current, such as voltage sags and fluctuations, transitory interruptions, harmonics, and oscillatory transients, producing failure, or maloperation of the power service equipment, are all examples of power quality problems. (Quirl et al., 2006)

Voltage sag and swell are the most common power quality issues impacting distribution networks, particularly in industries where losses can be quite severe. A dropout of an entire industry can be caused by a short and shallow voltage sag. In general, voltage sag and swell can be blamed for 10 to 90% of power quality issues (Pakharia & Gupta, 2012). Faults and short circuits, lightning strokes, and inrush currents are the most common sources of voltage sag. A single line-to-ground fault on the system might induce a transient voltage increase on the unfaulted phases and is also a common cause of voltage sag. As for voltage swell, it is usually caused by the switching off of large loads and the energization of capacitor banks.

Therefore, by knowing the causes of the voltage sag and swell, it also reduces the impact of power quality disturbance on the user as well. Studies have shown that one of the impacts is that sensitive electronic and electrical equipment may be subjected to failure, complete shutdown, or generate a large inrush current that results in blown fuses and tripped circuit breakers due to voltage sag and swell. Sensitive loads like PLC need a high-quality power supply. These power quality issues can cause serious malfunctions and lost production in industries. Also, it could fail or shut down, as well as create a large current unbalance that could blow fuses or trip breakers. These impacts can be very expensive for the customer, ranging from minor quality variations to production downtime and equipment damage (Francis & Thomas, 2014).

In this study, a simple control strategy by using the Proportional Integral–Grey Wolf Optimizer (PI-GWO) was designed to mitigate the voltage sag and swell that

happen during single-phase weak grid-connected conditions. The main purpose of mitigating the voltage sag and swell in weak grid conditions is to stabilise or restore the power quality back to its standard values in the power system right before it is transmitted to the end-user of electricity. With this, it helps to avoid transmitting poor power quality that might cause malfunctions or damage the equipment that requires a high quality of power supply.

1.3 Objectives of study

The main objectives of this study are:

1. To mitigate voltage sag and swell during weak grid conditions using PI-GWO.

2. To analyse the effectiveness of the proposed system under different percentages of voltage sag and swell.

1.4 Scope of project

The following scope of project will be performed in order to achieve the objectives as stated above.

1. To model a 5 MW photovoltaic system using Matlab Simulink.

2. To develop GWO algorithm for mitigating voltage sag and swell.

3. To analyse the dynamic behaviour of the system under different percentage of voltage sag and swell.

CHAPTER 2

LITERATURE REVIEW

2.1   Introduction

This chapter discusses the previous study of voltage sag and swell mitigation methods that are related to this project. There are various methods to mitigate the voltage sag and swell, whereas the mitigation methods can be divided into two categories: external devices and modified internal controllers. As shown in Figure 2.1, external devices are further classified as Flexible Alternating Current Transmission System (FACTS) interline Dynamic Voltage Restorer (DVR), DVR, enhanced DVR, series voltage regulator, distributed generation, and PWM - switched transformer. Ant Colony Optimization (ACO) with Distributed Power Flow Controller (DPFC), Moth Flame Optimization (MFO), Fuzzy based Particle Swarm Optimizer (PSO), Proportional-Integral (PI) controller, Distributed Generation (DG) using Genetic Algorithm (GA), and Grey Wolf Optimizer (GWO) are the modified internal controllers.
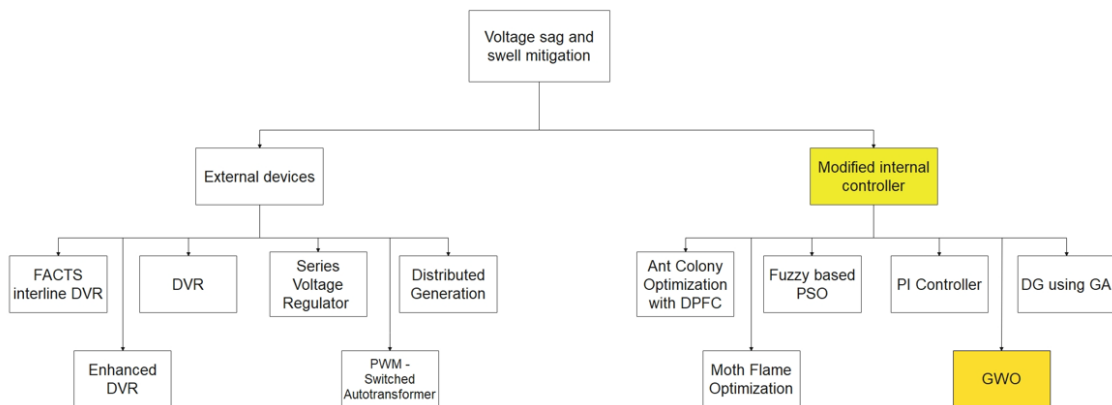
Figure 2.1   Voltage sag and swell mitigation method breakdown structure

2.2 External devices

External devices, also known as custom power devices, were introduced by N. G. Hingorani (N. G. Hingorani, 1995). The term "external devices" refers to future value-added electricity that electric utilities and other service providers will supply to their customers. The improved level of reliability of this power, in terms of fewer interruptions and less variation, will result from an integrated solution to current problems, with the application of power electronic controllers to utility distribution systems or the supply ends of many industrial and commercial customers and industrial parks being a prominent feature (Ghosh & Ledwich, 2002).

2.2.1 Flexible Alternative Current Transmission System (FACTS) Device Interline Dynamic Voltage Restorer (IDVR)
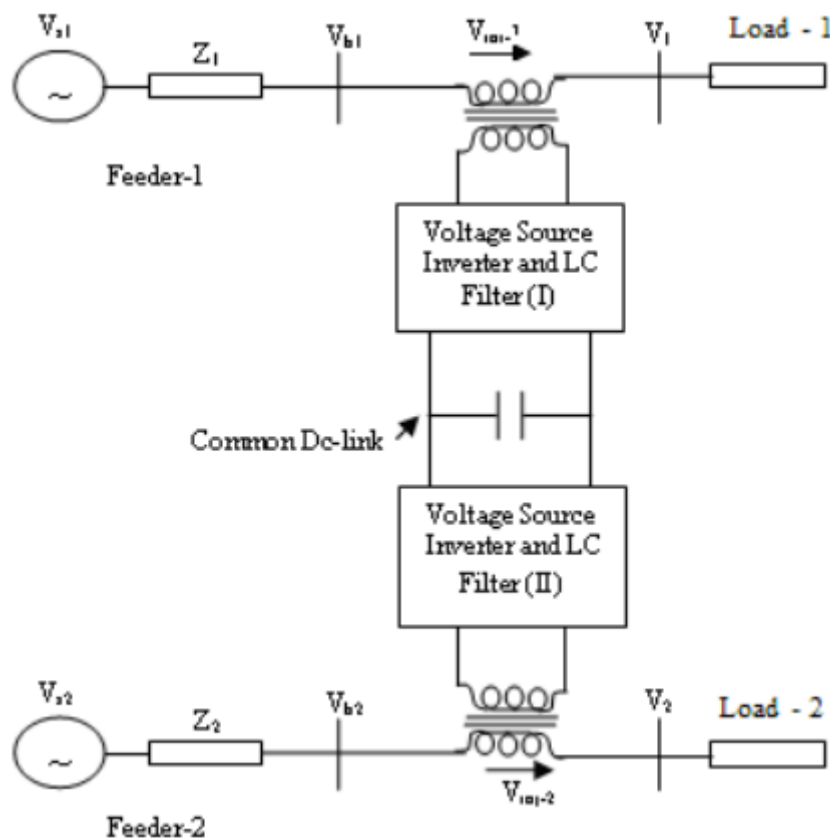
Figure 2.2   Interline dynamic voltage restorers (Dhas & Prakash, 2011)

Figure 2.2 illustrates the connection of the based mitigation device with converter in a series configuration. Voltage sag can be mitigated by using DVR and IDVR restorers.

The amount of stored energy within the restorer is one of the primary elements that limits the DVR's ability to compensate for long-duration voltage sags. To solve this issue, IDVR was proposed, which consists of two DVRs connected by a shared dc-link, each compensating a transmission line by series voltage injection. When one DVR compensates for voltage sag, the IDVR's dc-link energy storage is replenished by the other DVR (Dhas & Prakash, 2011).

2.2.2 DVR

The DVR is an effective option for reducing voltage fluctuations. It is a power electronics-based system that compensates for sag by providing power to sensitive loads. The DVR must use control loops to monitor the load voltage and provide adjustment during the sag. Those control loops must be fine-tuned using a mathematical model, performance requirements, and a thorough controller design technique (Francis & Thomas, 2014; Meloni et al., 2016).
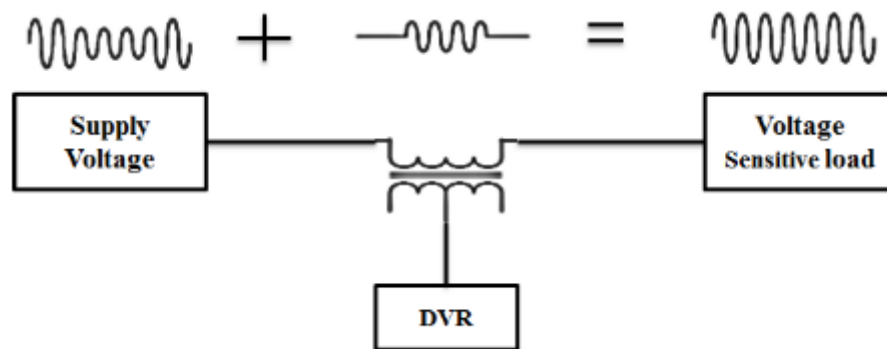
Figure 2.3   The operation of DVR (Francis & Thomas, 2014)

The basic idea of DVR operation is that it injects a voltage waveform that is the difference between pre-sag and sagged voltage through an injection transformer. Figure 2.3 illustrates the structure of the operation of DVR. DVR is made feasible by supplying the requisite real or active power as well as reactive power from an energy storage device. The maximum injection capability of DVR may be limited by the injection transformer ratio and the energy storage rating of device.

2.2.3   An Enhanced DVR
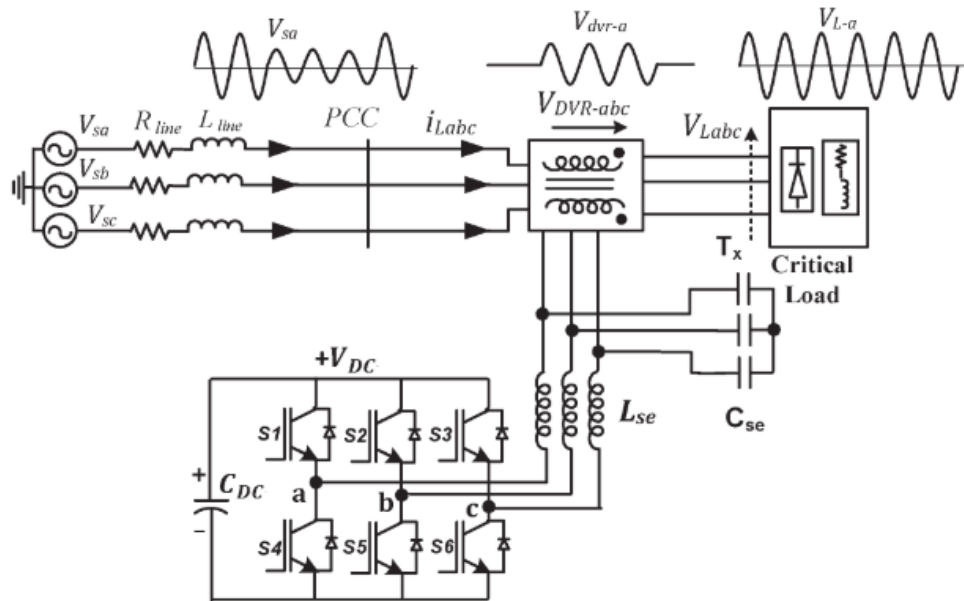
Figure 2.4   The configuration of enhanced DVR (Rauf & Khadkikar, 2015)

Figure 2.4 shows the configuration of an enhanced DVR that includes the dc-link capacitor. Enhance DVR is described as employing an upgraded DVR to improve the voltage quality of sensitive loads and protect them from voltage sags. The increased active power required for voltage phase jump adjustment has resulted in a significant increase in the size and cost of DVR's dc link energy storage system. The proposed enhanced sag compensation technique reduces the phase jump in the load voltage while improving the overall sag compensation time. When compared to existing phase jump compensation methods, an analytical investigation demonstrates that the suggested solution greatly increases DVR sag support time (by more than 50%). This improvement can also be observed as a significant reduction in the size of the DC link capacitor for new installations (Rauf & Khadkikar, 2015).

2.2.4 Pulse Width Modulation (PWM) – Switched Autotransformer
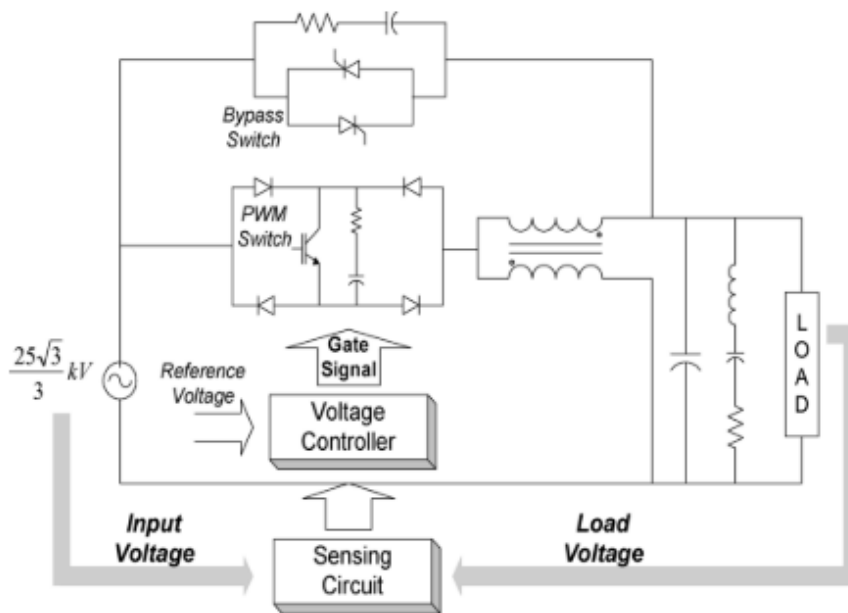
Figure 2.5   Basic configuration of PWM - switched autotransformer voltage compensation scheme (Lee et al., 2004)

Error! Reference source not found. shows the proposed scheme for the basic configuration of the PWM – switched transformer for voltage compensation. The PWM switched autotransformer is introduced here in order to attain the benefits of a fast response time at a much lower cost. The basic configuration of the PWM - switched autotransformer voltage compensation scheme is shown in Figure 2.5. It consists of a bridge configuration comprising a single PWM insulated gate bipolar transistor (IGBT), a thyristor by-pass switch, output filters, an autotransformer, and the system controller. With only one PWM switch per phase and no energy storage, the suggested system is a very low-cost approach for voltage sag mitigation. Any high-voltage power electronic switch is expensive, and peripheral circuits like gate drivers and power supplies are significantly more so. The total cost of power electronics-based equipment is almost linearly proportional to the total number of switches in the circuit topology (Lee et al., 2004).

2.2.5   Series Voltage Regulator
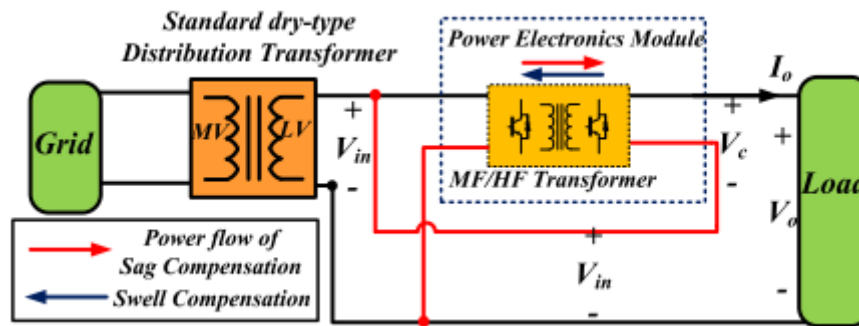
Figure 2.6   Scheme of the series voltage regulator on distributed transformer (Kang et al., 2017)

Figure 2.6 illustrates the configuration of a series voltage regulator with power electronic modules applied into a distributed transformer. A line frequency transformer is coupled to a power electronic converter, which is auto-connected on the secondary side, to build a series voltage regulator for a distribution transformer system. The use of a high-frequency or medium-frequency transformer facilitates this auto-connection. By offering continuous ac voltage control, a simplified technique to correct for voltage sags and swells on the grid side can be implemented. When a voltage sags or swells, the power electronic converter provides a compensating voltage that is vector-added to the grid voltage to adjust the output voltage to the load (Kang et al., 2017).

2.3   Internal modified circuit

Voltage sag and swell mitigation can be done through the optimization technique, which only requires the modification of the circuit to quality issues. Unlike external devices as mentioned before, optimization techniques can be easily installed inside the circuit with the aid of an algorithm to identify the quality issues and solve the problem by identifying the optimal solution to mitigate the voltage sag and swell.

2.3.1   Ant Colony Optimization (ACO) with Distributed Power Flow Controller (DPFC)

The DPFC is achieved by incorporating the two approaches (the deletion of the common Direct Current (DC) connection and the distribution of the series converter) into the Unified Power-Flow Controller (UPFC) as shown in Figure 2.7. The DPFC, like the

UPFC, is made up of shunt and series-linked converters. The shunt converter is comparable to a STATCOM, but the series converter uses the dye-sensitized solar cell (DSSC) principle, which uses numerous single-phase converters instead of a single three-phase converter.
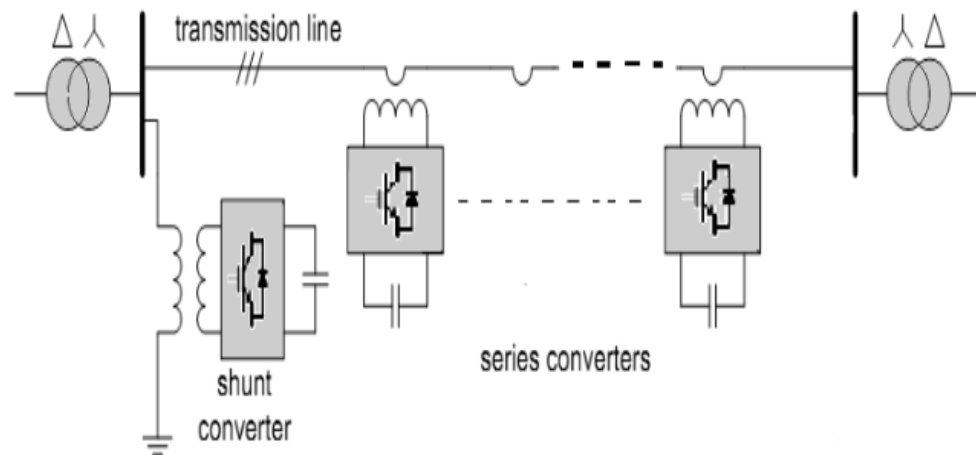
Figure 2.7   DPFC structure (Gopinath, 2016)

Figure 2.7 shows the DPFC structure that is used for mitigating the voltage sag and swell. One of the advantages of using DPFC is that all aspects of the transmission network can be controlled by the DPFC, including line impedance, transmission angle, and bus voltage magnitude. In terms of high reliability, the redundancy of series converters improves DPFC dependability during converter operation. It means that even if one of the series converters fails, the others can keep working. Lastly, the cost of applying DPFC is low, whereas in comparison to three-phase converters, single-phase converters have a very low rating. Furthermore, no voltage isolation is required to connect the series converters in line in this configuration. Single-turn transformers can be used to hang series converters. The use of linguistic variables rather than numerical ones distinguishes ACO as one of the most successful fuzzy set theory procedures. It gives a straightforward method for reaching a firm conclusion based on confusing, imprecise, noisy, or missing input data (Gopinath, 2016).

2.3.2   Levy Flight - Moth Flame Optimization (LFMFO)

MFO is a new meta-heuristic optimization method that was inspired by moths and their unique night navigation methods. They navigate using a technique known as transverse orientation. The Levy flight was invented in 1937 by Paul Levy, a French

mathematician. Levy flight is a statistical explanation of motion that goes beyond the more typical Brownian motion, which was discovered over a century ago. The optimization algorithm is improved by using the levy flight. The light is related to the Levy flying function of the MFO. As a result, levy flights have been included in the MFO method for optimization and optimal search. The Levy flight is used to improve MFO operations in order to find the optimum option for reducing PQ difficulties in smart grids (SG) based on the Suja research paper (Suja, 2021).
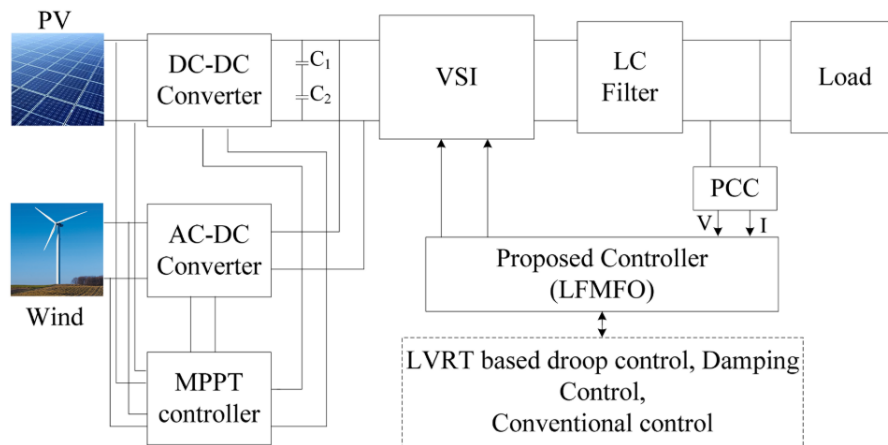
Figure 2.8   Block diagram of LFMFO method (Suja, 2021)

Figure 2.8 shows a model that is mostly utilised for MPPT technologies that employ the proposed methodology. A photocurrent, a diode, a parallel resistor expressing a leakage current, and a series resistor representing an internal resistance to the current flow are represented in the equivalent circuit of the general model. The LFMFO controller is shown in closed loop as feedback for the proposed system in the block diagram (Suja, 2021).

2.3.3   Fuzzy based Particle Swarm Optimizer (PSO) Controller

When judgement capabilities are required, fuzzy-based controllers outperform logical operators. The data parameter and the rule parameter are two interconnected and dependent elements. The elements are chosen because they have an important influence in determining capabilities. A fuzzy control system creates an automatic search and commands considerable control based on voltage drooping at the voltage supply point. The numerical values that the fuzzy model is built on are determined by the rule define parameter. PSO considers acceleration constant selection, inertia weights, and maximal

velocity restrictions for swarm augmentation and particle convergence in order to provide the best solution. PSO is given with non-linear inertial weight and changing coefficients in the PI controller, as well as enhanced gain parameters adjustment. As a result, in the performance index, the objective function was reduced with error criteria (Sudharani & Godwin Immanuel, 2021).

2.3.4 Proportional-Integral (PI) Controller

According to Ali Mohamed Eltamaly, the DVR can be adjusted to reduce the response time to the sag condition in the power system by using the PI control technique with the DVR control application in series or shunt controller. The temporal delay is treated using a weighted sum of the error, which is the difference between the actual sensed output and the integral value, by the PI controller (Mohamed Eltamaly et al., 2019).

2.3.5 Optimal Allocation of Distributed Generation (DG) using Genetic Algorithm (GA)

According to Mahda Jenabali Jahromi, the term "DG" refers to the deployment of any modular technology to improve service quality throughout a utility's service area (interconnected to the distribution or sub-transmission system). Improvements in power quality indices and growing requirements for high reliability have focused interest on DG to achieve satisfactory reliability when combined with the grid, and DG units are closer to customers, avoiding or reducing transmission and distribution (T & D) costs, these are the main reasons for the increasing widespread use of DG. GA is a class of computing models that are based on evolutionary notions. It is a well-known truth that, according to natural selection, only those people who are better adapted to their environment will survive and pass on their genes to future generations over the course of multiple generations (g, 1993). A new approach based on a GA is capable of determining the appropriate DG allocation on a medium-voltage (MV) distribution network while considering the system's vulnerability to voltage sag (Jena et al., 2007).

2.3.6 Grey Wolf Optimizer (GWO)

The Grey Wolf Optimizer is based on Seyedali Mirjalili's official account (Mirjalili et al., 2014), and a meta heuristic approach was developed in 2014. It mostly

replicates the hunt for prey, as well as surrounding and attacking prey. They have a highly tight social dominating hierarchy, as shown in Figure 2.9. The highest hierarchy is starts from alpha (α), beta (β), and delta (δ). The other wolves are identified as omega (ω). As shown in the GWO algorithm, the hunting or optimization is initiated by the alpha wolf and followed by the other wolves.
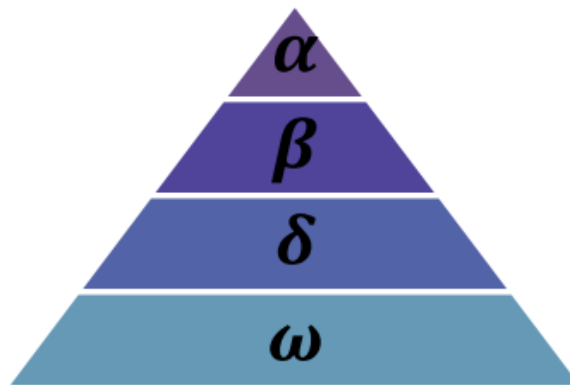
Figure 2.9   Hierarchy of grey wolf (Mirjalili et al., 2014)

Grey wolves engage in group hunting, which is an interesting social characteristic in addition to their social hierarchy. According to C. Muro (Muro et al., 2011), the following are the main phases of grey wolf hunting:

- The prey is tracked, chased, and approached.

- The prey is pursued, encircled, and harassed until it cannot move anymore.

- The prey is attacked.

To build GWO and perform optimization, this mathematically pursued style and the social hierarchy of grey wolves are represented in this work.

CHAPTER 3

METHODOLOGY

3.1   Introduction

This chapter will explain the methodology used to develop a single-phase grid-connected of PV system. It consists of modelling PV array by using mathematical equations in MATLAB Simulink. The SunPower 210 W Solar Panel is used as a reference model in the proposed system. Also, the size of the PV array run in the simulation is 5 MW. The PV array is then connected to a full bridge inverter, which is known as a DC-AC converter, before being connected to the grid system.

3.2   Block Diagram of the System
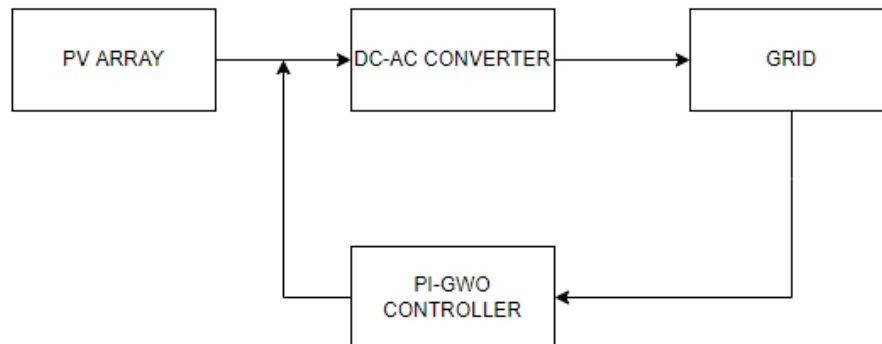
Figure 3.1   Block diagram of the system

The block diagram of a single-phase grid-connected system is shown in Figure 3.1. The modelling and simulation of the PV array is carried out in the MATLAB Simulink environment. The PV array, which is the power source or generator of light energy, is the fundamental configuration of the system. PV arrays were organised in series or parallel to maximise the benefits of solar radiation. Under varying working circumstances of solar

cells, a DC/DC converter is supplied to adjust the constant output voltage. The DC/AC inverter circuit is connected to a grid through a conventional step-up transformer.

3.3   Mathematical Equation Modelling for Equivalent Circuit of PV Array

Figure 3.2 shows the PV cell equivalent circuit. In the circuit, it includes a diode, a shunt resistor, a series of resistors, and a current diode source.
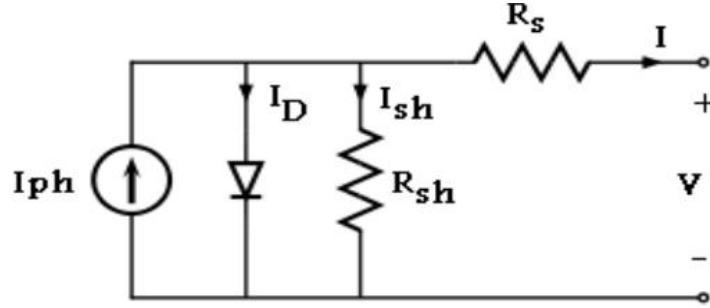
Figure 3.2   Equivalent circuit of PV cell (Salmi et al., 2012)

Cell photocurrent is represented as the current cell, I_{ph}, while R_{sh} and R_s are the intrinsic shunt and series resistance of the solar cell, respectively. Therefore, since the values for both , R_{sh} and R_s were very large and very small, both values may be neglected to simplify the analysis of PV cells. PV cells merged as a group in large quantities, to form what are called PV modules, which are further interconnected circuits in a configuration of parallel-series to form the PV array.

The model mathematically of the PV panel as given in equations (Chowdhury et al., 2008; Jung & Ahmed, 2010; Nguyen & Nguyen, 2015; Pandiarajan & Muthu, 2011; Premkumar et al., 2020; Salmi et al., 2012; Singh & Rajput, 2016).

Module photo-current:

$$I_{ph} = [I_{sc} + K_i(T - 298)] \times \frac{I_r}{1000} \qquad 3.1$$

Here;

I_{sc} : short-circuit current (A)

K_i : short-circuit current of cell at 25 °C and 1000 W/m^2

T : operating temperature (K)

I_r : Solar radiation (W/m^2)

Module reverse saturation current:

$$I_{rs} = \frac{I_{sc}}{exp\left(\frac{qV_{oc}}{N_s knT}\right) - 1}$$

3.2

Here;

q : electron charge = $1.6 \times 10^{-19} \, C$

V_{oc} : open-circuit voltage (V)

N_s : number of cells connected in series

k : Boltzmann's constant = $1.3805 \times 10^{-23} \, J/K$

n : ideality factor of the diode

The module saturation current varies with the cell temperature:

$$I_o = I_{rs} \left[\frac{T}{Tn}\right]^3 exp\left[\frac{qE_{g0}}{nk}\left(\frac{1}{T} - \frac{1}{Tn}\right)\right]$$

3.3

Here;

Tn : nominal temperature = $298.15 \, K$

E_{g0} : band gap energy of the semiconductor = $1.1 \, eV$

The current output of PV module:

$$I = N_p \times I_{ph} - N_p \times I_o \times \left[exp\left(\frac{\frac{V}{N_s} + I \times \frac{Rs}{N_p}}{n \times V_t}\right)\right]$$

3.4

With

$$V_t = \frac{k \times T}{q}$$

3.5

And

$$I_{sh} = \frac{V \times \frac{N_p}{N_s} + I \times R_s}{R_{sh}}$$

3.6

Here;

N_p : Number of PV modules that connected in parallel configuration

R_s : value of series resistance (Ω)

R_{sh} : value of shunt resistance (Ω)

V_t : diode thermal voltage (V)

3.4   Reference Model of PV

The 210 W solar power module is used as the simulation's reference module, and the module's exact specifications are listed in Table 3.1.

Table 3.1   The data of electrical characteristic of SPR-210-BLK-U PV module

Parameter	SPR-210-BLK-U
Peak Power (P_{max})	210 W
Rated Voltage (V_{mpp})	40.0 V
Rated Current (I_{mpp})	5.25 A
Open Circuit Voltage (V_{oc})	47.7 V
Short Circuit Current (I_{sc})	5.75 A
Total number of cells in series	72
Total number of PV modules in parallel	1
Maximum system voltage	600 V
Range of operation temperature	-40 °C to 80 °C

3.5   Step by Step Procedure of PV Module Modelling using MATLAB Simulink

Iph=[Isc+Ki*(T-298)]*(G/1000)
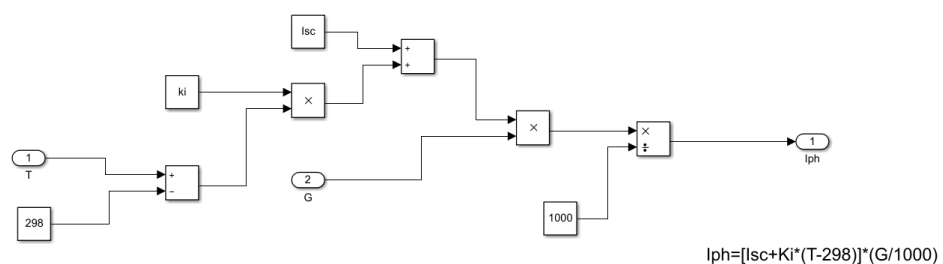
Figure 3.3   Model circuit for equation 3.1

Figure 3.4 shows the module photo-current based on Equation 3.2. The module photo-current is the generation of the current based on the irradiance of the sunlight encountered by the PV.
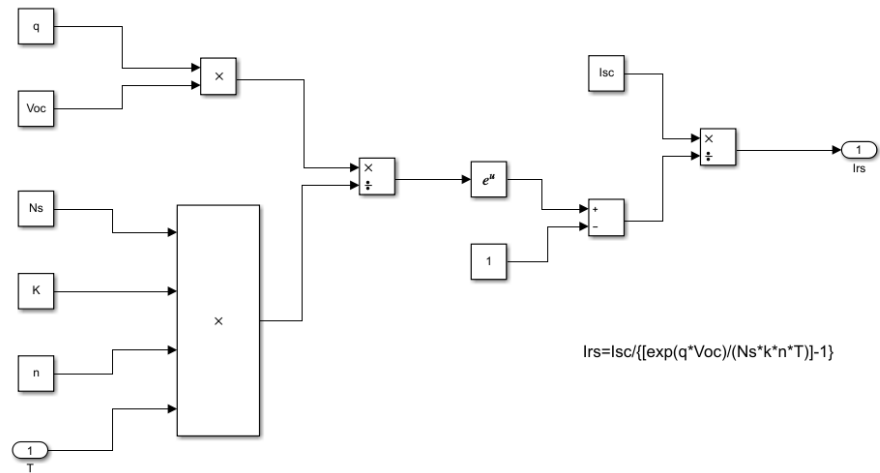
Figure 3.4   Model circuit of equation 3.2

Figure 3.4 shows the module of reverse saturation current based on Equation 3.3. In reverse saturation current, the connection between the electron charge, the open-circuit voltage of the PV array, and the number of cells of PV in series.
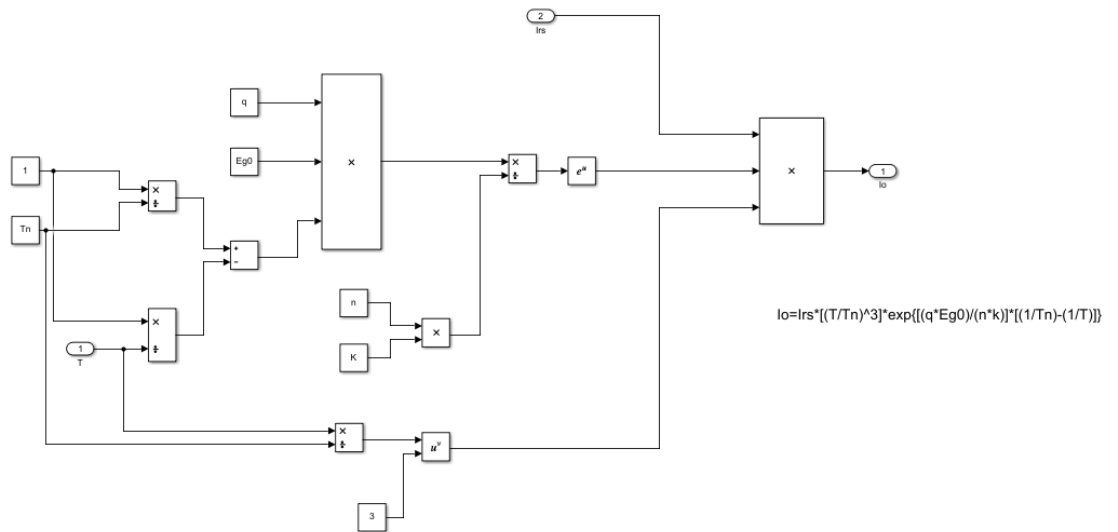
Figure 3.5   Model circuit for equation 3.3

Figure 3.5 shows the module saturation current varies with the cell temperature based on Equation 3.3. The connection of the module shared with the value of reverse saturation current and temperature of the PV array as external inputs. Then it involves the specified nominal temperature, Boltzmann's constant, and electron charge constant.

19
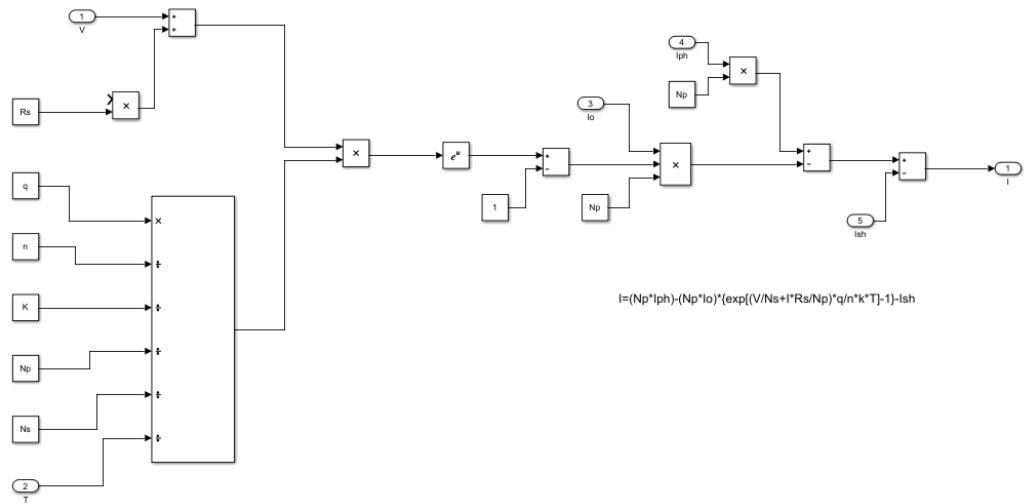
Figure 3.6   Model circuit for equation 3.4

Figure 3.6 shows the current output of the PV module. In this model, the electron charge, number of series and parallel PV cells, and ideal factor of diode are connected with the temperature of the PV, value of the resistance, and value of shunt current to produce the current output of PV.
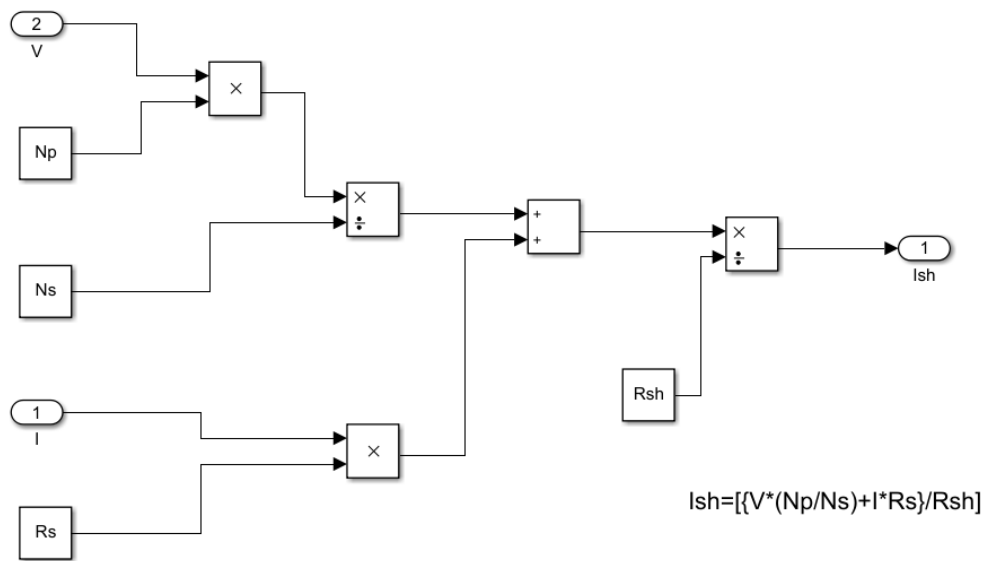
Figure 3.7   Model circuit of equation 3.6

Figure 3.7 shows the model of shunt current. External connections from voltage and current are connected with the number of series and parallel PV cells, and the value of the resistance to produce the shunt current.
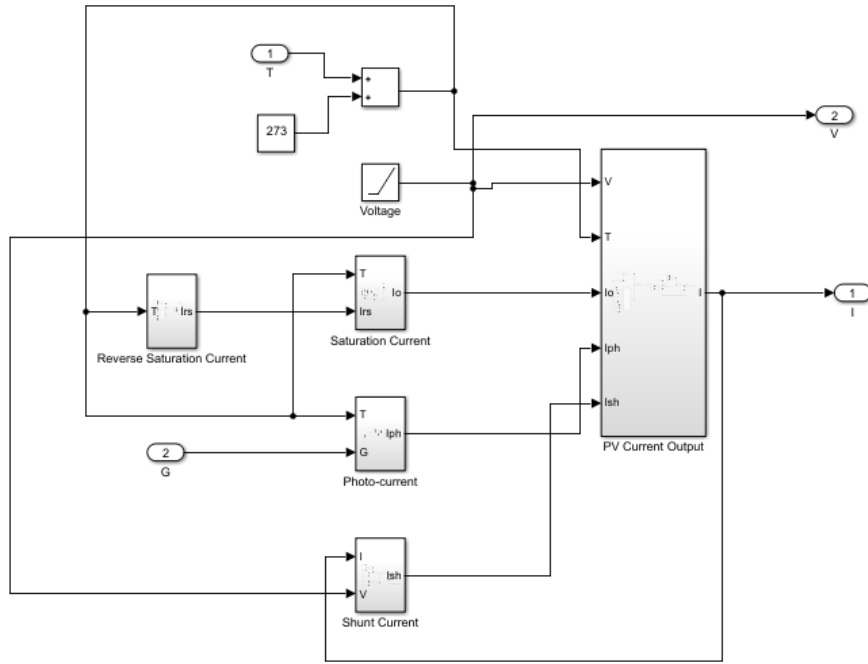
Figure 3.8   Interconnection between 5 subsystems

Figure 3.8 shows the connection between the five sections that developed based on the mathematical equation to produce a PV array. The output of this connection is the current output of the PV array.
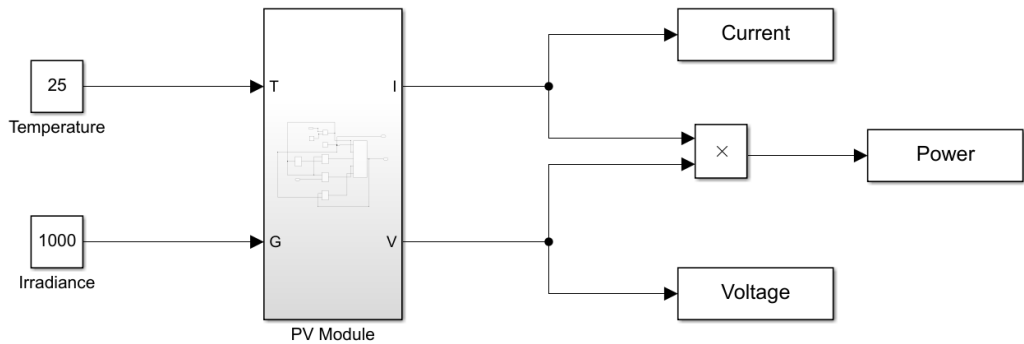
Figure 3.9   PV model

Figure 3.9 shows the final model of the PV model, whereas the saved workspace is included in the model to measure the value of voltage, current, and power. It takes operating temperature in Celsius and irradiance as input values and will give both values of output current and voltage to create I-V curve and P-V curve characteristics.

3.6 Development of a Single-Phase Grid-Connected System

Figure 3.10 illustrates the construction of a single-phase grid-connected PV system. A PV array, a DC-AC converter, and a PI controller with unipolar pulse width modulation (PWM) are all provided. The voltage and current controllers use PI controllers. The DC-AC converter is a device that converts a DC power source to an AC power source. AC oscillates around a 0V base level, commonly in a square or sinusoidal pattern, whereas DC is a relatively steady and positive voltage source. The PWM circuit function is to turn the PI controller's control signal into a switching signal.
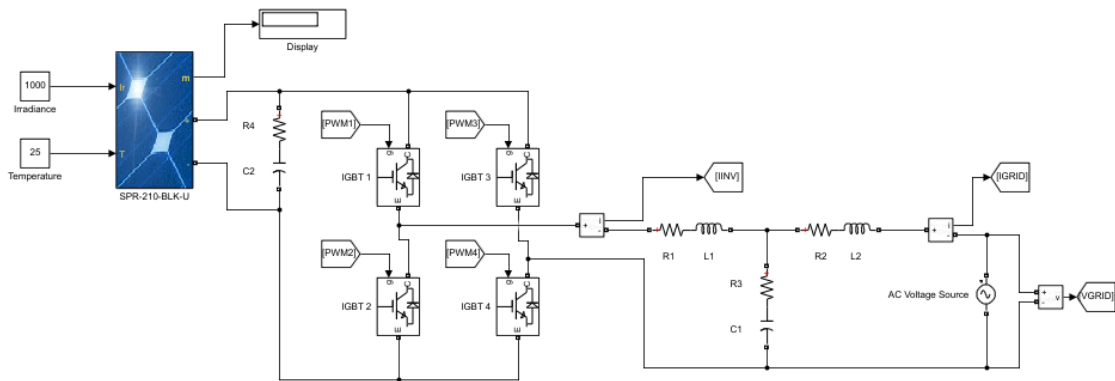
Figure 3.10   Single-Phase Grid-Connected System Simulation

A single SunPower SPR-210-BLK-U module can only generate 210 W, according to Table 3.1. As a result, to increase current and voltage, the PV module must be linked in parallel and series configurations. The voltage increases when PV cells are connected in series, so the current also increases when PV cells are connected in parallel. A 5 MW PV system is made up of 41 series modules with 582 parallel strings, as demonstrated in the following calculation:

$$41 \ series \ module \ \times I_{mpp} = 215.25 \ A$$
$$582 \ parallel \ string \ \times V_{mpp} = 23280 \ V$$
$$215.25 \ A \ \times 23280 \ V = 5011020 \ W \qquad \qquad 3.7$$

Figure 3.10 also illustrates the assembly of a bridge inverter. IGBT1, IGBT2, IGBT3, IGBT4, and a load resistor RL make up the bridge inverter circuit. To efficiently convert DC to AC, the four IGBTs were coupled in a closed-loop arrangement. It is accomplished

by opening and shutting the switches in the proper sequence. This inverter features a variety of operational modes that are dependent on closed switches.

Table 3.2   IGBT parameters

IGBT	Internal resistance Ron (Ohms)	Snubber resistance Rs (Ohms)
IGBT 1	1e−3	1e5
IGBT 2	1e−3	1e5
IGBT 3	1e−3	1e5
IGBT 4	1e−3	1e5

Table 3.3   Resistor parameter

Resistor	Resistance (Ohms)
R1	0.001
R2	0.001
R3	0.0042
R4	0.0042

Table 3.4   Inductor parameter

Inductor	Inductance (H)
L1	4.06e−3
L2	4.35e−3

Table 3.5   Capacitor parameter

Capacitor	Capacitance (F)
C1	6.01e−6
C2	500e−6

Table 3.2 shows the parameters of four IGBTs used in the development of bridge inverters to change DC power supplies to AC power supply. Table 3.3, Table 3.4, and Table 3.5 are the values of resistors, inductors, and capacitors that are used in the design of single-phase grid-connected PV systems. In a DC circuit, capacitors operate as an insulator. They are ideal for high-frequency signal transmission. For a DC circuit, inductors serve as conductors. They excel at transmitting low-frequency signals while filtering out high-frequency signals and oscillations.

3.7   Voltage Sag and Swell Configuration

Figure 3.11 shows the configuration of the voltage sag and swell that occur within 0.15 s and 0.43 s. An AC voltage source is connected to 2 inductors, then connected to the breaker to cause the voltage sag, before it ends the connection with the voltage grid at R5 and L3. The same goes for the voltage swell block. The subsystem consists of a breaker component and an AC voltage source to execute the voltage swell into the system output.
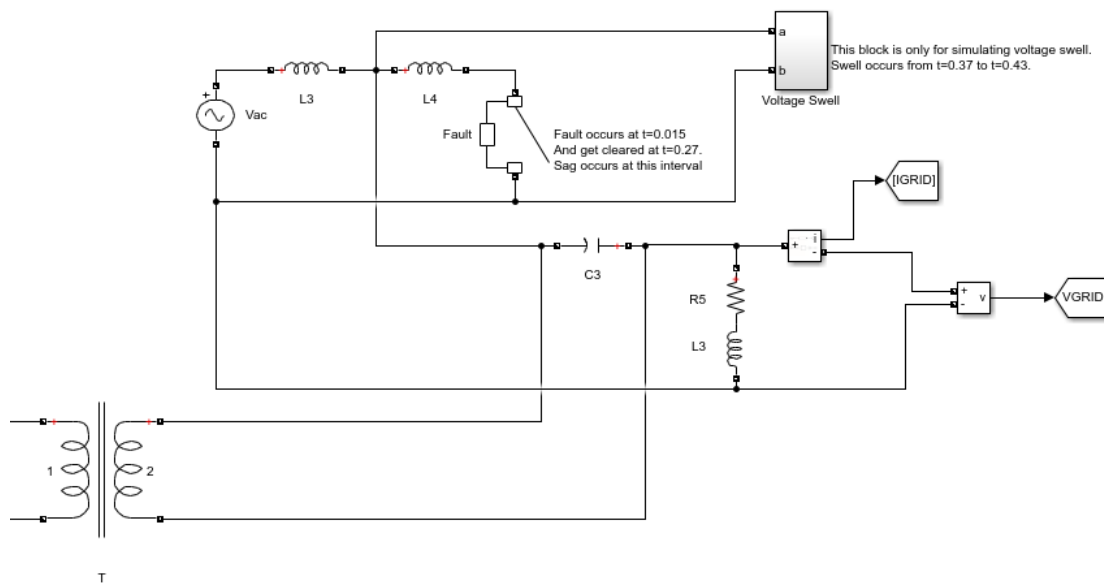
Figure 3.11   Voltage sag and swell configuration

The percentage of voltage sag can be increased by adjusting the value of breaker resistance at the voltage sag configuration part in order to achieve 10% and 20% of voltage sag. The value of voltage sag at 10% voltage drop is 216 V, whereas the value of voltage sag at 20% voltage drop is 192 V. These values can be seen at the voltage output of the single-phase grid-connected PV system.
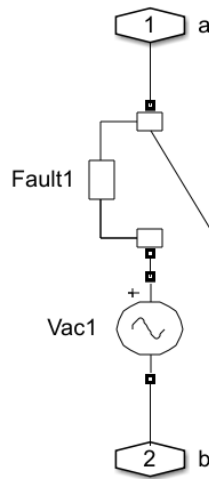
Figure 3.12   Voltage swell subsystem

Voltage swell can be increased by changing the parameters of the AC voltage source without changing the value of the resistance of the breaker. Figure 3.12 shows the connection between the AC voltage source and the breaker in order to create a voltage swell inside the system.

Table 3.6   Percentage of voltage sag

Voltage Sag (Percentage)	Parameters	
	AC Voltage Source (Voltage)	Breaker Resistance (Ohms)
10%	335	0.074
20%	335	0.048

Table 3.7   Percentage of voltage swell

Voltage Swell (Percentage)	Parameters	
	AC Voltage Source (Voltage)	Breaker Resistance (Ohms)
10%	375	0.01
20%	409	0.01

Table 3.6 and Table 3.7 are the parameters of AC voltage source and breaker resistance to config the percentage of voltage sag and voltage swell at 2 cases of voltage faults – 10% and 20%. .

3.8   Controller Development

A controller in a control system is a device that attempts to reduce the difference between a system's actual value (i.e., the process variable) and its desired value (i.e., the setpoint). All sophisticated control systems need controllers, which are a key aspect of control engineering. As a consequence, a controller is a device that is employed to regulate a process variable such as measurement. It monitors the error signal in real time and sends a corrected signal to the final control element.

3.8.1   PI Controller

A feedback control loop which is in PI controller able to calculate the error signal such as subtract the difference in between of a system desired output and the set point as the power drawn from the voltage reference. (Cherati et al., 2011)
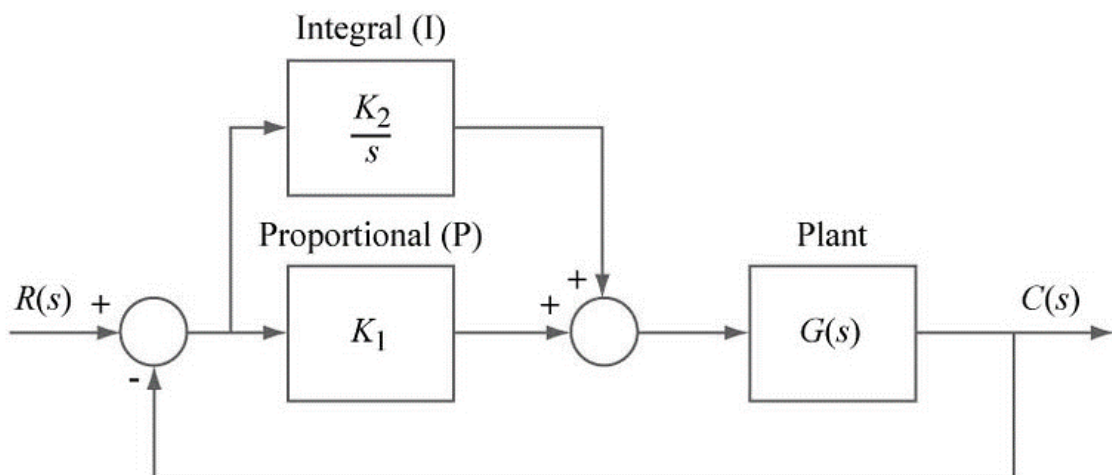
Figure 3.13   PI controller block diagram (Sule et al., 2020)

Figure 3.13 is the block diagram of the PI controller used in the single-phase grid-connected system. It's important to note that this is related to the complexity of the electronic components used in the single-phase grid-connected system. The parameters were determined by using the Ziegler-Nichols method. (Selvaraj & Rahim, 2009)

26
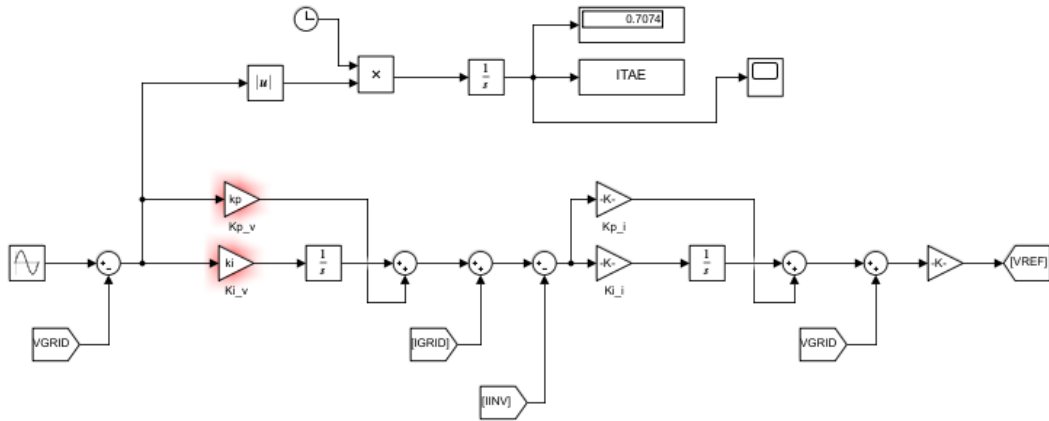
Figure 3.14   PI controller circuit

Figure 3.14 illustrates the design of the PI controller in Simulink that involves a voltage regulator, current regulator, and integral of time-weighted absolute error (ITAE). In the design of PI controllers, minimising ITAE is generally referred to as a favourable performance measure. The search for controller parameters may be achieved for certain types of loads and/or set point changes, and because this criterion is based on error computation, it can be simply applied to various processes characterised by various process models. The values of Kp and Ki for the voltage regulator part is the main focus for tuning the mitigation of voltage sag later. Meanwhile, Kp and Ki for the current regulator are ignored as they does not affect the voltage output of the system.
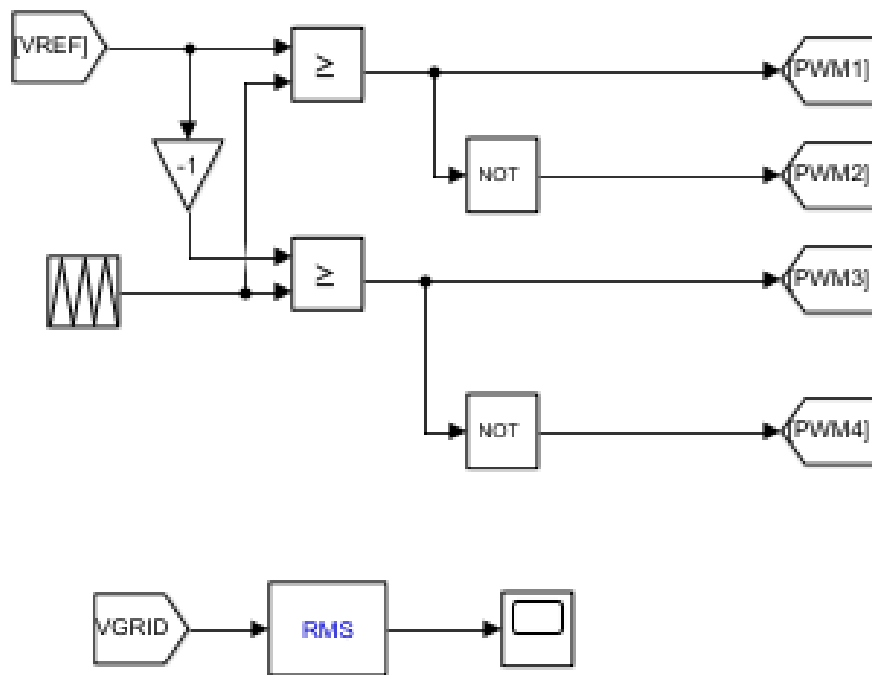
Figure 3.15   Unipolar PWM

Figure 3.15 shows the simulation of unipolar PWM. The PWM duty cycle signal is varied, resulting in voltages across the load that appear to the load as an AC signal in a specified pattern. After sending the signal via a low pass filter, the result is a pure sine wave. An analogue or digital microcontroller can be used to construct the pattern at which the duty cycle of a PWM signal fluctuates. The output of the inverter is controlled by sinusoidal PWM generated by any of the two main topologies. Unipolar PWM typically needs two sinusoidal modulated waves, vm and vm-, that are 180 degrees out of phase but have the same amplitude and frequency. In the positive half cycle of the fundamental frequency, the inverter's output voltage varies between zero and + Vd, and in the negative half cycle, it shifts between zero and -Vd, resulting in unipolar modulation. Overmodulation occurs when the amplitude modulation index ma is larger than 1. The number of pulses in the line-to-line voltage waveform is reduced, and the harmonics are reduced. Furthermore, in the middle of the positive and negative half cycles, the notch and pulse width tend to vanish. To complete the device switching process, the minimum blocking width and pulse width must be reached. When the notch and minimum width pulses are removed, the load current temporarily spikes. To modify the system output

voltage, the result of unipolar PWM is sent to the full bridge inverter of a single-phase grid-connected PV system.

3.8.2 PI-GWO Controller
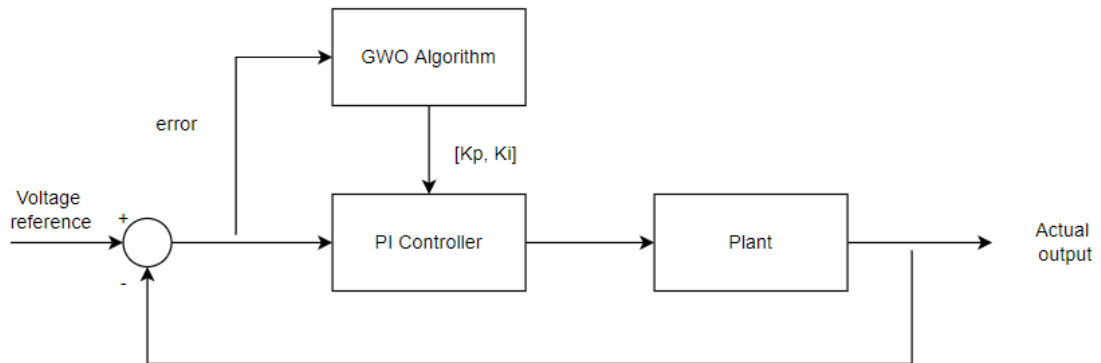
Figure 3.16   PI-GWO controller block diagram (Jaalam et al., 2022)

By referring to Figure 3.14, the values of proportional gain (Kp) and integral gain (Ki) are represented in the GWO algorithm. The tuning is done by running the simulation of the GWO algorithm, which is shown in Appendix 2. GWO starts it iteration until it achieves the number of iterations applied. The initialize parameters of GWO are stated as below.

- Number of search agents = 5

- Maximum iterations = 30

- Number of variables = 2

- Upper boundary = [150 5000]

- Lower boundary = [0 55]

The initial parameters are set based on the configuration of the PI controller which later on, the iterations will start to tune in the step response of the voltage regulator for both Kp and Ki by referring to the ITAE until it achieved the desired voltage output. The search agents repeat iterations once until all five search agents have updated their position in the algorithm, and then repeat iterations until it has completed the maximum number of iterations specified in the initial parameter.

3.9   Grey Wolf Optimization Algorithm System

Employ the best solution as the alpha (α) to mathematically characterise the social structure of wolves while building GWO. As a consequence, it will be followed by the second beta (β) and third delta (δ) best options, respectively. Omega (ω) is assumed to be the only remaining feasible pack. The optimization of the GWO algorithm is directed by the alpha wolf, beta wolf, and delta wolf. The wolves ω are on the lookout for these three wolves.

3.9.1   Encircling Prey

As previously stated, grey wolves will begin to encircle victims during the hunting process. The following equations are presented to mathematically model encircling behaviour:

$$\vec{D} = \left| \vec{C}.\overrightarrow{X_p}(t) - \vec{X}(t) \right| \qquad \text{3.8}$$

$$\vec{X}(t+1) = \overrightarrow{X_p}(t) - \vec{A}.\vec{D} \qquad \text{3.9}$$

where t is the current iteration, $\vec{A}$ and $\vec{C}$ denotes coefficient vectors, $\overrightarrow{X_p}$ denotes the position vector of the prey, and $\vec{X}$ denotes the position vector of a grey wolf. The vectors A and C are computed in the following way:

$$\vec{A} = 2\vec{a}.\overrightarrow{r_1} - \vec{a} \qquad \text{3.10}$$

$$\vec{C} = 2.\overrightarrow{r_2} \qquad \text{3.11}$$

where $\vec{a}$ components are linearly reduced from 2 to 0 across iterations, r_1 and r_2, are random vectors in the range [0,1]. A two-dimensional position vector and some of the potential companions are shown in Figure 3.17 to show the implications of equations (3.8) and (3.9). A grey wolf at the position of (X,Y) can change its position in response to the position of the prey (X*,Y*), as shown in the figure below.
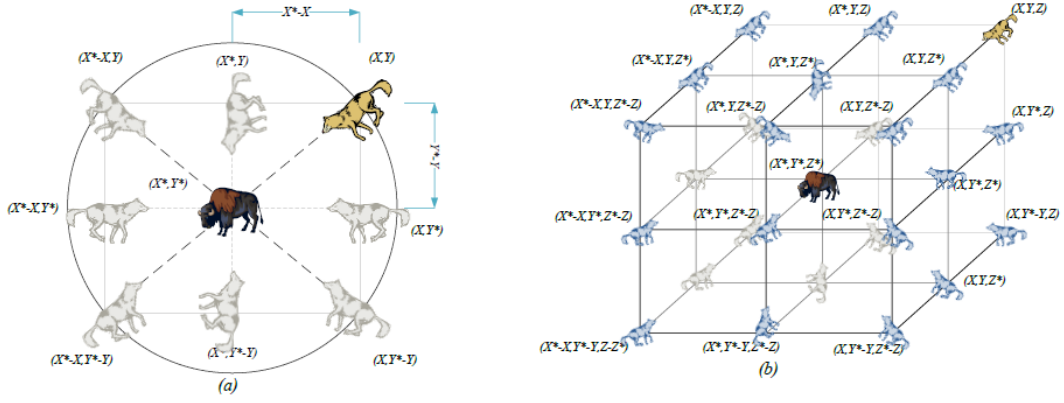
Figure 3.17   Position vectors and possible next location in 2D and 3D (Mirjalili et al., 2014)

By altering the values of $\vec{A}$ and $\vec{C}$ vectors, several locations around the best agent may be attained with respect to the present position. Setting $\vec{A}$ and $\vec{C}$, for example, will get it to (X*-X,Y*). Figure 3 illustrates the possible updated locations of a grey wolf in 3D space. It is worth noting that the random vectors r_1 and r_2 allow wolves to reach any spot between the positions shown in Figure 3.17. Using equations (3.8) and (3.9), a grey wolf may update its position inside the space around the prey at any random place.

3.9.2   Hunting

Grey wolves have the ability to track and encircle their prey. Most of the time, alpha is in charge of hunting. beta and delta may engage in some hunting from time to time. However, in an abstract exploring environment, you have no way of knowing where the greatest spot is. Alpha, beta, and delta seek to have a better understanding of prospective prey sites in order to simulate grey wolf hunting behaviour computationally. As a consequence, it keeps the top three best solutions found so far and pushes other Omega search agents to update their position to match the best search agent's location. For this, theoretically may use the following formula:

$$\overrightarrow{D_\alpha} = \left|\vec{C_1}.\overrightarrow{X_\alpha} - \vec{X}\right|, \overrightarrow{D_\beta} = \left|\vec{C_2}.\overrightarrow{X_\beta} - \vec{X}\right|, \overrightarrow{D_\delta} = \left|\vec{C_3}.\overrightarrow{X_\delta} - \vec{X}\right| \qquad 3.12$$

$$\overrightarrow{X_1} = \overrightarrow{X_\alpha} - \overrightarrow{A_1}.\left(\overrightarrow{D_\alpha}\right), \overrightarrow{X_2} = \overrightarrow{X_\beta} - \overrightarrow{A_2}.\left(\overrightarrow{D_\beta}\right), \overrightarrow{X_3} = \overrightarrow{X_\delta} - \overrightarrow{A_3}.\left(\overrightarrow{D_\delta}\right) \qquad 3.13$$

$$\vec{X}(t+1) = \frac{\overrightarrow{X_1} + \overrightarrow{X_2} + \overrightarrow{X_3}}{3} \qquad 3.14$$
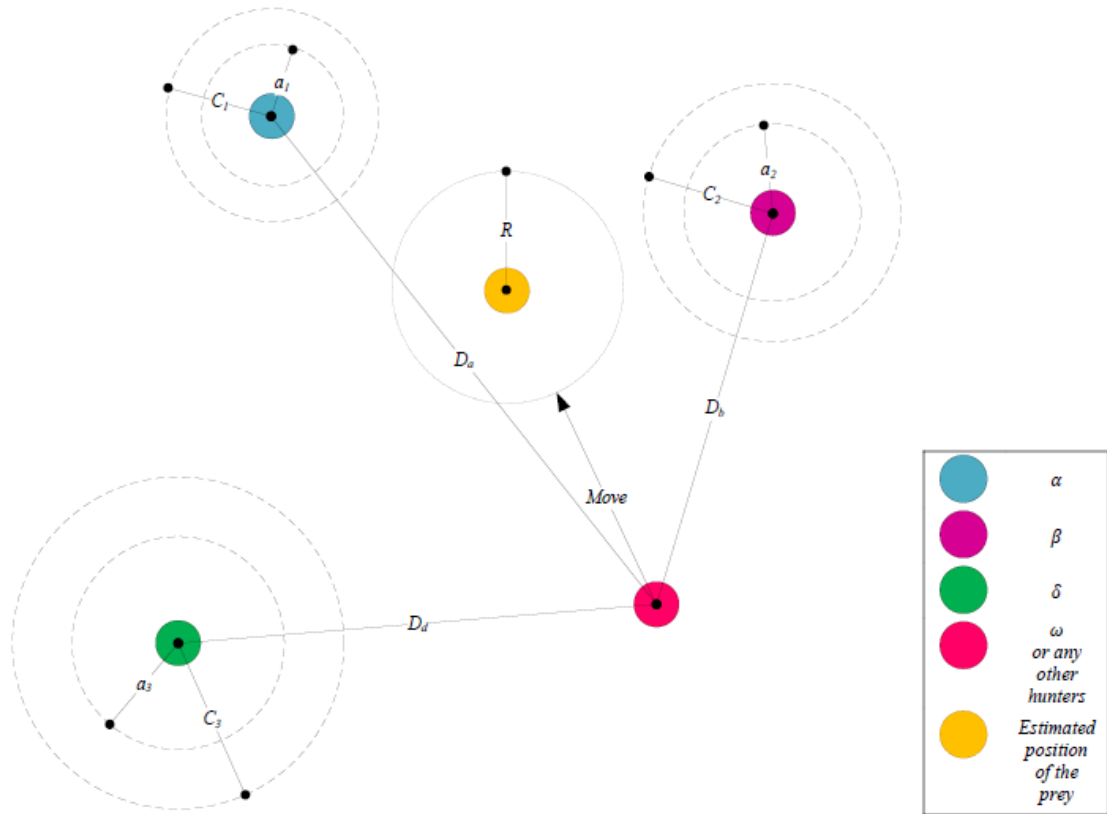
Figure 3.18   GWO position update (Mirjalili et al., 2014)

Figure 3.18 shows how a search agent modifies its location in a 2D search space based on alpha, beta, and delta. In the search space, the final position seems to be at a random place within a circle created by the locations of alpha, beta, and delta. To put it another way, alpha, beta, and delta estimate the location of the prey, while other wolves change their positions at random around it.

3.9.3   Exploitation

Grey wolves end the hunt by attacking the victim when it stops moving, as previously indicated. It happens by theoretically simulating approaching the prey by lowering the value of $\vec{a}$. It is important to note that A lowers $\vec{A}$ fluctuation range. In other words, $\vec{A}$ is a random variable having a decreasing value from 2 to 0 across repetitions in the range $[-a, a]$. A search agent's future position can be anywhere between its current position and the position of the prey when A has random values in the range [-1,1]. As seen in Figure 3.19, |A|<1 prompts the wolves to attack the prey.

32

Figure 3.19   Attacking and searching the prey (Mirjalili et al., 2014)

Figure 3.19 illustrate the direction of gey wolf when attacking and searching the prey. The GWO algorithm allows its search agents to update their position depending on the location of the alpha, beta, and delta, and assault towards the prey, using the operators described thus far. The GWO method, on the other hand, is prone to local solution stagnation when using these operators. True, the proposed encircling mechanism promotes exploration to some extent, but GWO need more operators that prioritise exploration.

3.9.4   Exploration

Grey wolves generally use the alpha, beta, and delta locations when searching. They split apart to hunt for prey before reuniting to attack it. To mathematically characterise divergence, they utilise $\vec{A}$ with random values which is greater than 1 or less than -1 to lead the search agent to diverge from the prey. This fosters experimentation and allows the GWO algorithm to search the whole world. Figure 3.19 shows that |A|>1 causes grey wolves to split out from their prey in the hopes of locating a better acceptable meal. Another GWO component that promotes experimentation is $\vec{C}$. As demonstrated in Equation (3.11), the $\vec{C}$ vector contains random values in the range [0, 2]. This component gives prey random weights to stochastically enhance (C>1) or deemphasize (C1) the importance of prey in determining distance in Equation (3.8). This allows GWO to act more erratically during optimization, encouraging exploration and avoiding local optima. It's worth noticing that, unlike A, C does not decrease in a linear fashion. We anticipate C to give some random values at all times, not only during the early rounds but even

during the last iterations, to encourage exploration. When local optima become stuck, especially in the last iterations, this component comes in helpful.

In nature, the C vector may also be thought of as the influence of barriers on approaching prey. In general, natural impediments exist in wolves' hunting pathways, preventing them from accessing prey swiftly and easily. This is precisely what the vector C accomplishes. Depending on a wolf's posture, the prey might gain weight and become tougher and farther to reach for wolves, or vice versa. To conclude, the search phase started with a random population of grey wolves generated by the GWO algorithm (potential solutions). During iterations, the alpha, beta, and delta wolves assess the likely whereabouts of the prey. Each probable optimizer distance from the prey is updated. The value of a is lowered from 2 to 0 to emphasise exploration and exploitation. Candidate solutions intend to disunite from the prey and close in on towards the prey when $|\vec{A}|>1$ and $|\vec{A}|<1$ is present. When an end condition is reached, the GWO algorithm is terminated.

3.9.5 GWO Algorithm
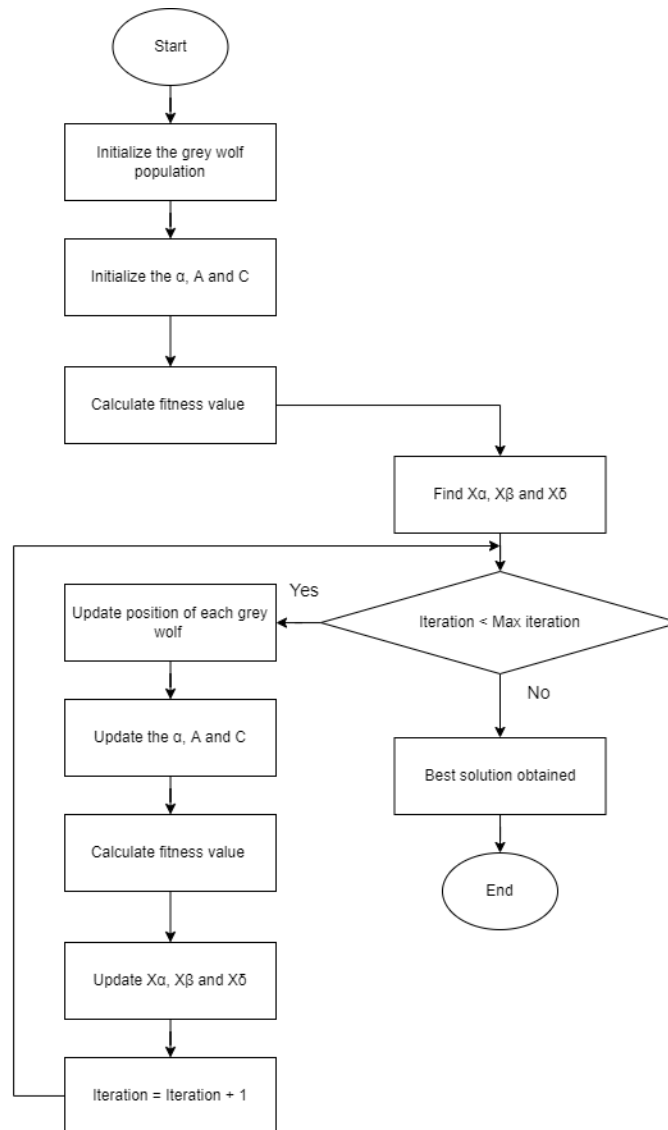
Figure 3.20   GWO algorithm

Figure 3.20 shows the flowchart of the GWO algorithm. The fittest option for representing the social behaviour of the grey wolf is alpha, which is followed by beta and delta, while the remainder of the solutions are categorised under omega. The hunting (optimization) process in GWO is directed by alpha, beta, and delta, with omega following these three wolves at all times. The search method begins with the GWO algorithm producing a random population of grey wolves. Then, the initial parameters, such as the number of iterations, number of variables, upper and lower boundary, and the objective function of the algorithm are set in the coding of the GWO algorithm. The number of variables is set to 2, because the variables that are used in the controller is Kp

and Ki. While for the upper and lower boundary, these two parameters indicate the values of Kp, and Ki are set from the lowest value to the highest value needed to tune the controller. An objective function is a function file that sets the objective of the algorithm, whereas for this project, the objective of the controller is to achieve the stabilization of voltage sag and swell at 240 V. These parameters are representing in α, A and C. Alpha, beta, and delta wolves evaluate the likely position of the prey during the period of iterations. The value of the best search agent for alpha, beta and delta obtained before it checks the number of iterations achieved or not. If the number of iterations does not achieve the maximum number of iterations, the algorithm will repeat itself by updating the position of the grey wolves and parameters of α, A and C. The distance between each possible solution and the prey is updated. In order to emphasise exploration and exploitation, the value of alpha is reduced from 2 to 0. When $|\vec{A}| > 1$, candidate solutions tend to disunite from the prey, but when $|\vec{A}| < 1$ they tend to close in on the prey. After that, the fitness value is calculated for each of the gey wolf in order to update the possible value of the best search agent of alpha, beta, and delta. Later, the number of iterations is added then the algorithm will be check back whether the number of maximum iterations has been achieved yet. Finally, when the execution requirements are met, the GWO algorithm is cancelled.

CHAPTER 4

RESULTS AND DISCUSSION

4.1   Introduction

In this chapter, the simulation of the PV model is developed and run with the help of equations under varying irradiation and constant operating temperature. The reference PV model used is SPR-210-BLK-U PV, as the data has been given by the panel manufacturer. The PV array is designed to produce a 5MW power output. Then, the voltage output of the single-phase grid-connected PV system produced 240V by using a linear transformer. The voltage sag and voltage swell are mitigated by using the PI-GWO controller to reduce the voltage drop and voltage rise of the single-phase grid-connected PV system.

4.2   5MW Photovoltaic Array Characteristics

As shown in Figures 4.1, the output characteristics of the I-V curve and the P-V curve of the PV module with various irradiation values and constant operating temperature are obtained as shown in Figures 4.1 and 4.2.
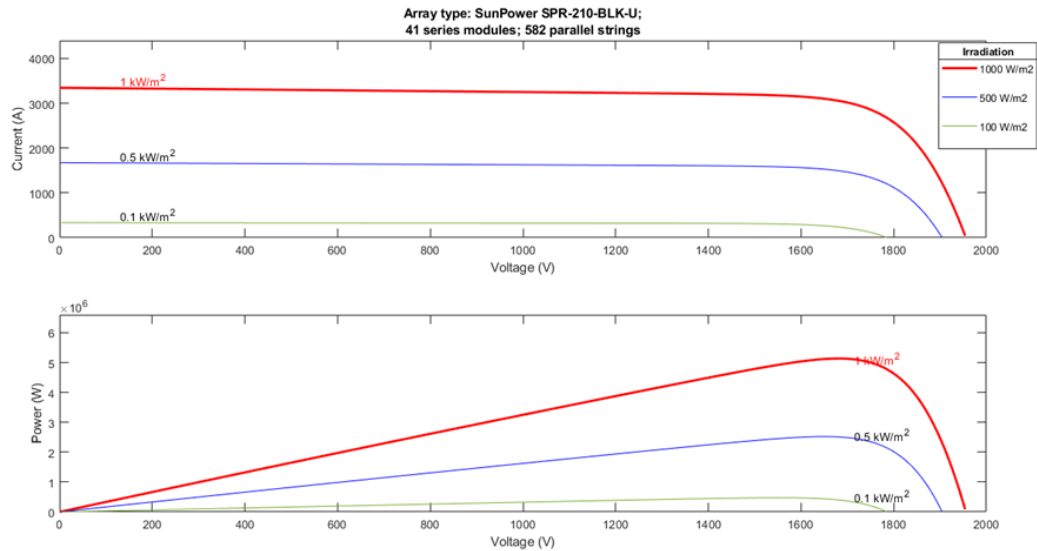
Figure 4.1   I-V and P-V characteristic

Figure 4.1 shows the few current and voltage output combinations that the PV array device may provide as the irradiance changes. The maximum voltage is reached when the circuit is broken. The voltage over an open circuit is referred to as "VOC." In this case, the resistance is infinitely high, and there is no current since the circuit is incomplete. On the (vertical) y-axis is current represented in amps. The (horizontal) x-axis represents voltage. The power available from a photovoltaic device at each point along the curve is just the product of current and voltage at that point. The power output is 0 V since the voltage is zero at the short circuit current point. At the open circuit voltage point, the power output is also 0 V, but this time because the current is also zero. There is a location around the curve's knee where the maximum power output is found. At this highest power point in Figure 4.1, the voltage is 23280 V and the current is 215.25 A. As a result, the maximum wattage is 5 MW. Aside from that, the P-V characteristics curves at a constant temperature of 25 C for varied solar irradiation intensities. The open circuit voltage decreases as the irradiation level decreases. The power output of PV by the defined model was more or less 5% off when compared to the rated power of PV modules by manufacturers on an average basis. The I-V and P-V characteristic curves produced from the proposed model matched the curves drawn from the PV module under standard test circumstances. The main source of fluctuations in PV module power production is revealed to be variations in incident solar radiation. A linear connection is discovered between the PV module's power output and the quantity of incident solar irradiation when all other factors are maintained constant.

4.3   Voltage Sag and Swell Characteristics

Voltage sags are classified by their size or depth, as well as their duration. A voltage sag occurs when the RMS voltage decreases between 10% and 90% of the nominal voltage for one-half cycle to one minute. According to some sources, a sag is described as a period of low voltage that lasts from 0.5 cycle to a few seconds, but a persistent sag is defined as a period of low voltage that lasts for an extended period of time. According to IEEE 1159, 3.1.73, a deviation in the RMS value of the voltage from the nominal voltage for a time more than 0.5 cycles of the power frequency but less than or equal to one minute. Typically, a modifier defining the magnitude of a voltage change is included in the description.

IEEE 1159 defines voltage swell as a rise in the RMS voltage level to 110%-180% of nominal during half cycle to one minute at the power frequency. It's classified as a short-term voltage fluctuation phenomenon, one of the key types of power quality difficulties covered in the second instalment of this site's power quality basics series.
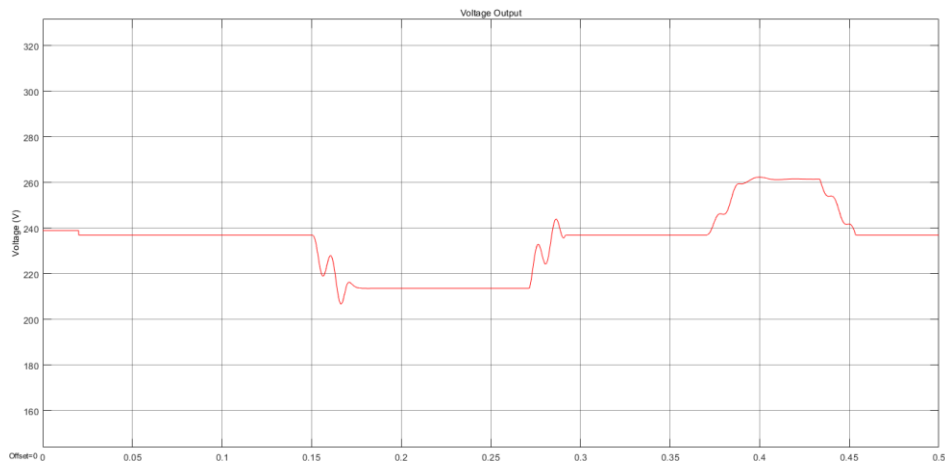

Figure 4.2   10% of voltage sag and swell
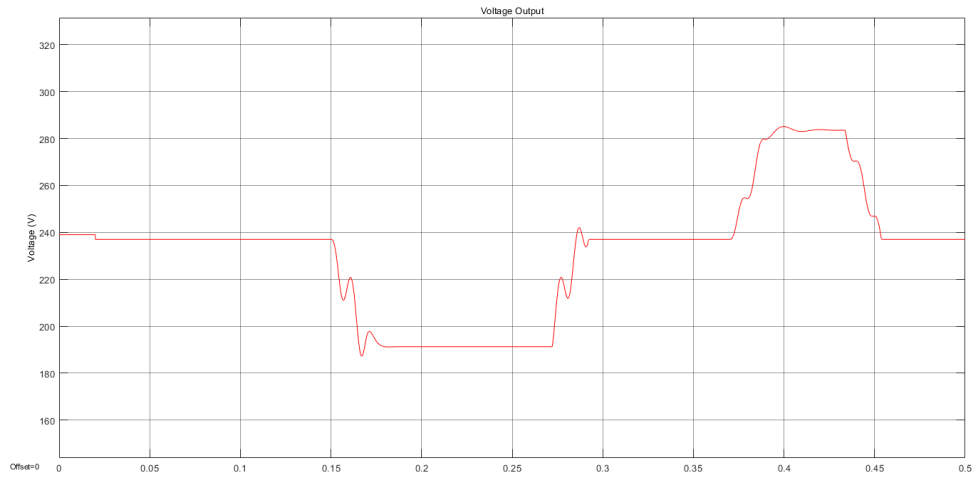
Figure 4.3   20% of voltage sag and swell

Voltage sag and swell are configured as shown in Figure 3.11 to achieve 10% and 20% of voltage drop and voltage rise, respectively. The value of 10% voltage sag and swell is 216V and 264V, respectively. Meanwhile, the value of 20% voltage sag and swell is 192V and 288V, respectively. The voltage output of voltage sag and swell for both cases – 10% and 20%, is shown in Figure 4.2 and Figure 4.3.

4.4   Mitigation of Voltage Sag and Swell

To mitigate the voltage sag and swell, the PI controller can be used to reduce the voltage drop and voltage rise, which can be seen in the voltage output of the single-phase grid-connected PV system. Therefore, two controllers' voltage sag and swell mitigation – PI controller and the PI-GWO controller, as the result will be compared at the end of the simulation. Two case studies were done using MATLAB and Simulink software to assess the effectiveness of the recommended control technique: one with a 10% voltage drop and rise, and one with a 20% voltage drop and rise, both with a single-phase fault and load power quality interruption. Between 0.15 and 0.27, the voltage sag fault occurred, and between 0.37 and 0.43, the voltage swell fault occurred.

4.4.1 Mitigation of Voltage Sag and Swell at 10%

Figure 4.4   Mitigation of voltage sag and swell at 10%

At 10% of voltage sag and swell, it shows that the mitigation has been done in both situations. For voltage sag, the initial voltage output before mitigating by PI and PI-GWO controllers is 216.4V. The number of iterations is 30 for the 10% voltage drop case, and the number of search agents is 5. Figure 4.5 illustrates the convergence curve for this simulation, with 0.99228 as the most optimum value of the objective function determined by the GWO. The optimum answers obtained by GWO after optimization are 13 and 442.7999, which is the optimal value for Kp and Ki. Figure 4.4 compares the voltage sag profiles of systems with PI-GWO, PI only, and systems without PI. The voltage was effectively increased to 223.9V and 231.9V using PI and GWO-PI based controllers, as both controllers were able to minimise the voltage sag by lowering the voltage drop from 10% to 2.97%.

Figure 4.5   Convergence curve for 10% voltage sag

The initial voltage output of voltage sag before been mitigating by PI and PI-GWO controllers is 263.9V for voltage swell. For the 10% voltage rise case, the number of iterations is 30 and the number of search agents is 5. The convergence curve for this simulation is shown in Figure 4.6, with 2.6464 as the most optimal value of the GWO-determined objective function. The best values for Kp and Ki are -5.2718 and 78.1282, respectively, as determined by GWO following optimization. The voltage swell profiles of systems with PI-GWO, PI, and systems without any controller are compared in Figure 4.4. Using PI and GWO-PI based controllers, the voltage was efficiently reduced to 260.3V and 256V, as both controllers were able to reduce the voltage swell by decreasing the voltage drop from 10% to 7.11%.

Figure 4.6   Convergence curve for 10% voltage Swell

4.4.2   Mitigation of Voltage Sag and Swell at 20%
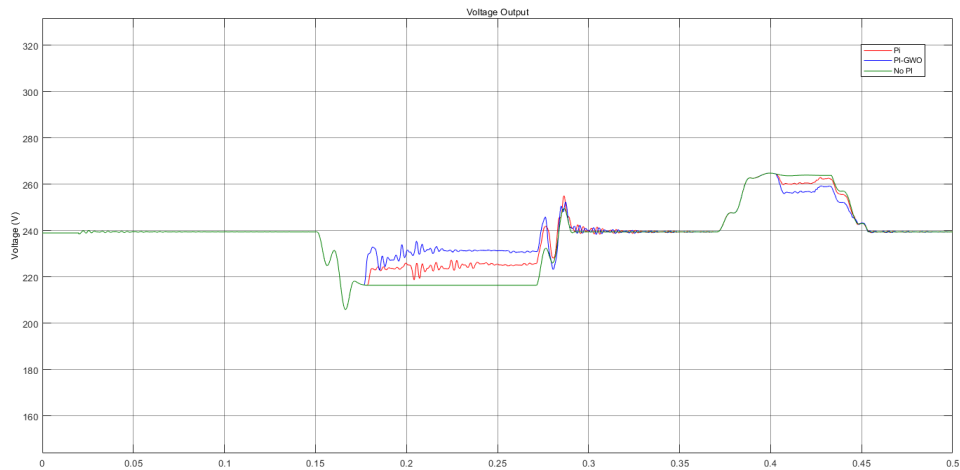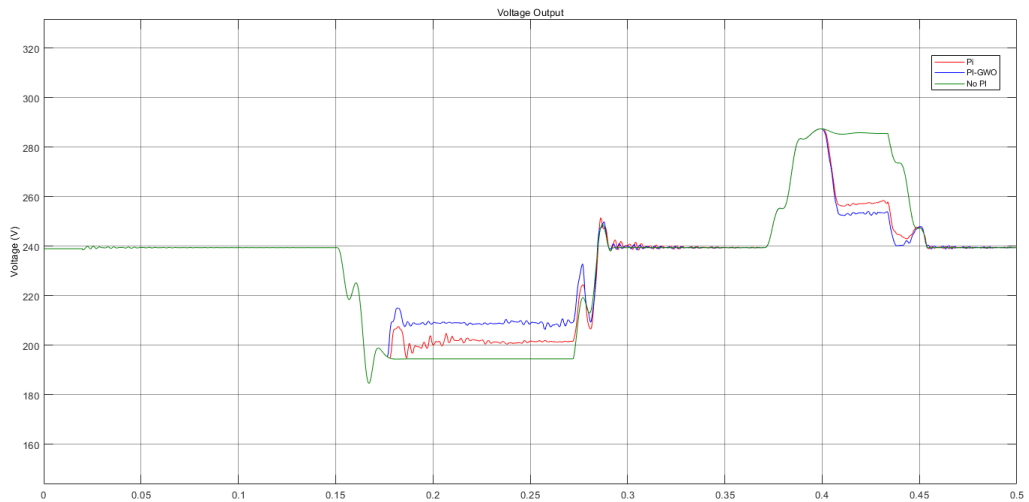

Figure 4.7   Mitigation of voltage sag and swell at 20%

At 20% of voltage sag and swell, it shows that the mitigation has been done in both situations. For voltage sag, the initial voltage output before mitigating by PI and PI-GWO controllers is 194.5V. The number of iterations is 30 for the 10% voltage drop case, and the number of search agents is 5. Figure 4.8 illustrates the convergence curve for this simulation, with 2.7945 as the most optimum value of the objective function determined

by the GWO. The optimum answer obtained by GWO after optimization is 100 and 492.7988, which is the optimal value for Kp and Ki. Figure 4.7 compares the voltage sag profiles of systems with PI-GWO, PI only, and systems without PI. The voltage is effectively increased to 201.3V and 218.7V using PI and GWO-PI based controllers, as both controllers were able to minimise the voltage sag by lowering the voltage drop from 20% to 8.49%.
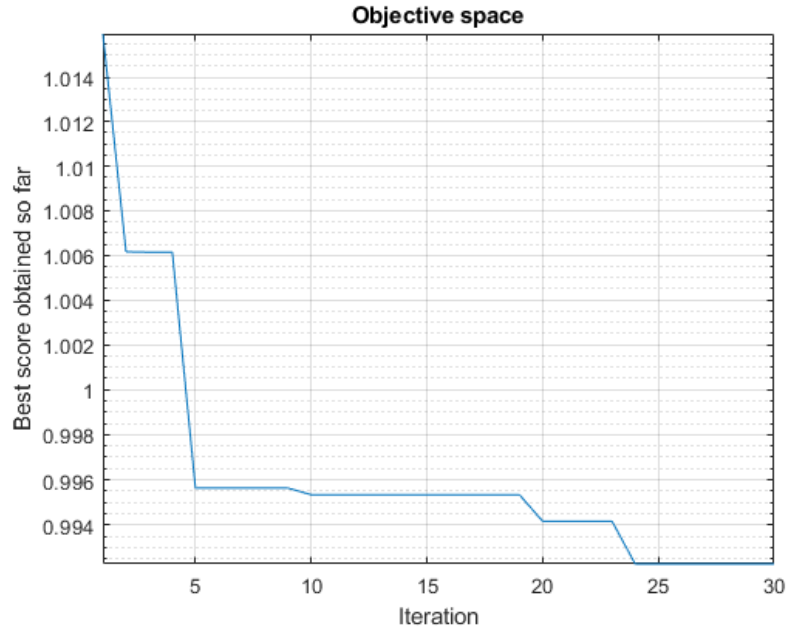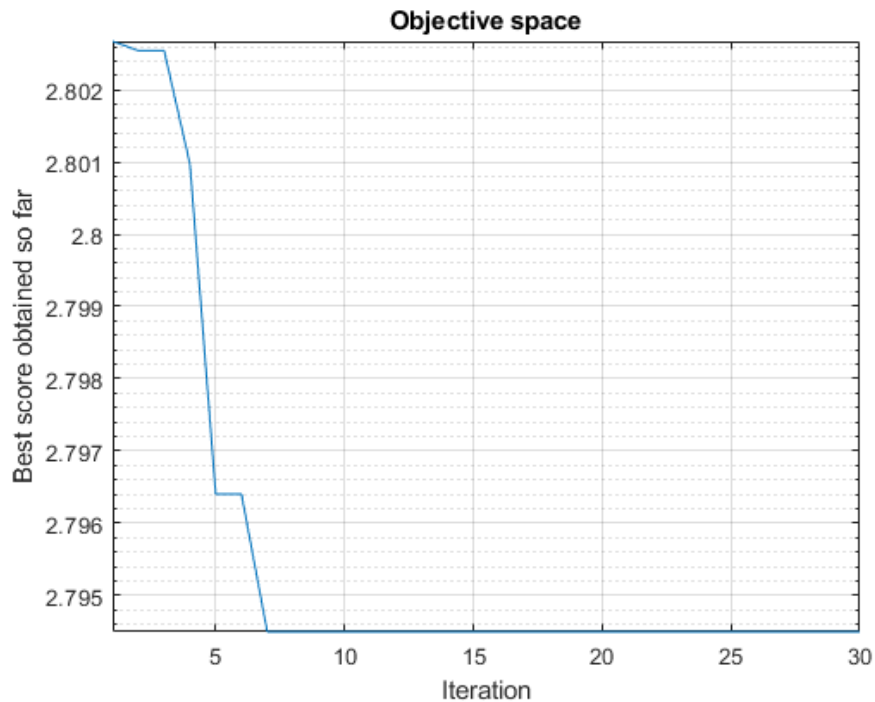

Figure 4.8   Convergence curve for 20% voltage sag

The initial voltage output of voltage sag before been mitigated by PI and PI-GWO controllers is 285.5 V for voltage swell. For the 10% voltage rise case, the number of iterations is set to 30 and the number of search agents is set to 5. The convergence curve for this simulation is shown in Figure 4.9, with 1.40119 as the most optimal value of the GWO-determined objective function. The best values for Kp and Ki are -12.4826 and 349.7209, respectively, as determined by GWO following optimization. The voltage swell profiles of systems with PI-GWO, PI only, and systems without PI are compared in Figure 4.4. Using PI and GWO-PI based controllers, the voltage was efficiently reduced to 260.3V and 256V, as both controllers were able to reduce the voltage swell by decreasing the voltage drop from 10% to 7.11%.
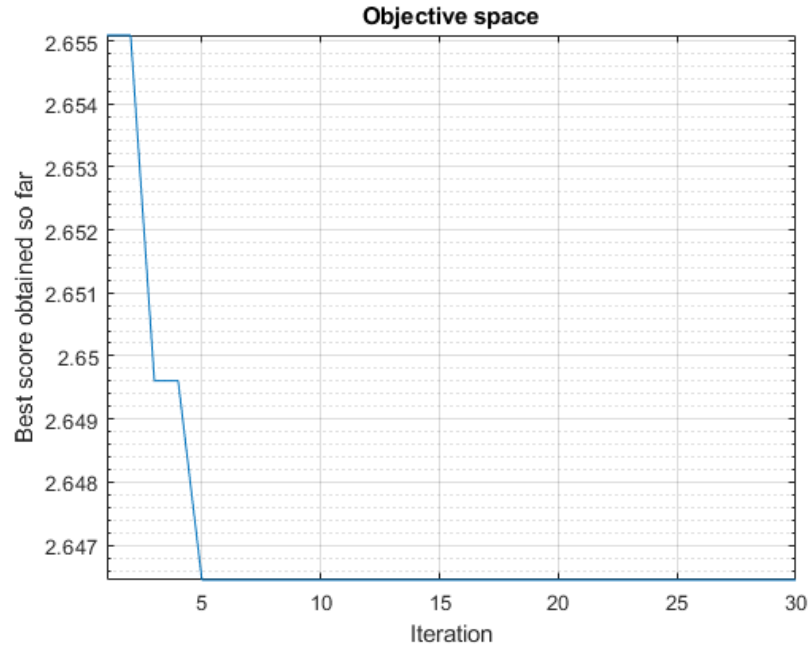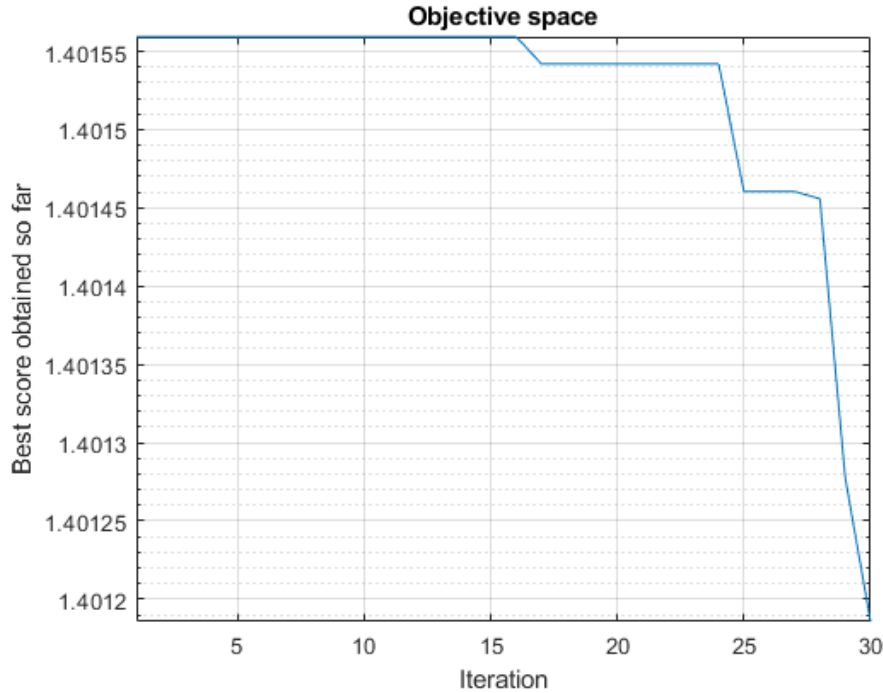
Figure 4.9   Convergence curve for 20% voltage swell

4.4.3   Comparison between the PI and PI-GWO Controller

Table 4.1   Controller comparison at 10% voltage sag

Voltage Sag	No PI	PI	PI-GWO
Voltage Output (V)	216.4	223.9	231.9
Percentage Drop (%)	9.5	6.32	2.97

Based on Table 4.1, the differences of percentage drop appear to have been reduced when mitigation occurred. When using a PI controller, the value of the percentage drop was reduced from 9.5% to 6.32%. But, when using PI-GWO controller, the reduction of percentage drop is greater than using the PI controller only, which is from 9.5% to 2.97%. Hence, the voltage output of the system can avoid the voltage sag power quality issue. Although the mitigation does not meet 0% voltage drop, there is an improvement in mitigating the voltage sag by using the PI-GWO controller.

Table 4.2   Controller comparison at 10% voltage swell

Voltage Swell	No PI	PI	PI-GWO
Voltage Output (V)	263.9	260.3	256
Percentage Rise (%)	9.6	8.91	7.11

Table 4.2 shows that when mitigation occurs, the variations in percentage rise appear to decrease. When the PI controller is used, the percentage decrease was lowered from 9.6% to 8.91%. However, when the PI-GWO controller was used instead of the PI controller alone, the percentage rise was reduced by more, from 9.5 % to 7.11 %. As a result, the voltage output of the system can avoid the voltage swell power quality issue. While the mitigation does not achieve a 0% voltage drop, the PI-GWO controller does enhance the voltage swell mitigation.

Table 4.3   Controller tuning for 10%

Comparison		PI	PI-GWO	Objective Space
Voltage Sag	Voltage Output (V)	223.9	231.9	
	Kp	9.2107	13	0.99228
	Ki	55	442.7999	
Voltage Swell	Voltage Output (V)	260.3	256	
	Kp	-4.058	-5.2718	2.6464
	Ki	55	78.1282	

The comparison tuning of PI and PI-GWO is shown in Table 4.3. Based on the values of Kp and Ki, it shows that when there is a 10% voltage sag, the PI tuning was 9.2107 and 55 to mitigate the voltage sag. Then, the PI-GWO controller has a higher value of Kp and Ki compared to the PI controller, which was 13 and 442.7999. Therefore, it was proven that in order to mitigate the voltage sag and achieve less than 3% of voltage drop, it requires much greater values of Kp and Ki in the voltage regulator to reduce the voltage sag amplitude. So, the best optimal value of the objective function found by GWO for voltage sag was 0.99228. When it comes to voltage swell, the values of Kp and Ki reveal that the PI tuning for mitigating was -4.058 and 55 when there was a voltage rise. Then, when compared to the PI, the PI-GWO has lower Kp and greater Ki values of -5.2718 and 78.1282, respectively. As a result, it has been demonstrated that in order to mitigate voltage swell and achieve a voltage rise of less than 8%, lower values of Kp and greater Ki in the voltage regulator are required to lessen the voltage swell amplitude. So, the best optimal value of the objective function found by GWO for voltage swell was 2.6464.

Table 4.4   Controller comparison at 20% voltage Sag

Voltage Sag	No PI	PI	PI-GWO
Voltage Output (V)	194.5	201.3	218.7
Percentage Drop (%)	19.96	15.77	8.49

Based on Table 4.4, the differences in percentage drop appear to have been reduced when mitigation occurred. When using a PI controller, the value of the percentage drop was reduced from 19.96% to 15.77%. But, when using the PI-GWO controller, the reduction of percentage drop was greater than when using the PI controller alone, which was from 19.96% to 8.49%. Hence, the voltage output of the system can avoid the voltage sag power quality issue. Although the mitigation does not meet 0% voltage drop, there was an improvement in mitigating the voltage sag by using the PI-GWO controller.

Table 4.5   Controller comparison at 20% voltage swell

Voltage Swell	No PI	PI	PI-GWO
Voltage Output (V)	285.5	258.3	252.6
Percentage Rise (%)	19.46	8.075	5.69

Table 4.5 shows that when mitigation occurs, the variations in percentage rise appear to decrease. When the PI controller was used, the percentage decrease was lowered from 19.46% to 8.06%. However, when the PI-GWO controller was used instead of the PI controller alone, the percentage rise was reduced by more, from 19.46% to 5.69%. As a result, the voltage output of the system can avoid the voltage swell power quality issue. While the mitigation does not achieve a 0% voltage drop, the PI-GWO controller does enhance the voltage swell mitigation.

Table 4.6   Controller tuning for 20%

Comparison		PI	PI-GWO	Objective Space
Voltage Sag	Voltage Output (V)	201.3	218.7	
	Kp	80.5691	100	2.7945
	Ki	52.354	492.7988	
Voltage Swell	Voltage Output (V)	258.3	252.6	
	Kp	-8.15	-12.4826	1.40119
	Ki	67.813	349.7209	

The comparison between the PI controller and the PI-GWO controller was shown in Table 4.3. Based on the values of Kp and Ki, it shows that when there was a 20% voltage sag, the PI tuning was 80.5691 and 52.354 to mitigate the voltage sag. Then, the PI-GWO controller has a higher value of Kp and Ki compared to the PI controller, which was 100 and 492.7988. Therefore, it was proven that in order to mitigate the voltage sag achieve achieve less than 9% voltage drop, it requires much greater values of Kp and Ki in thevoltage regulator to reduce the voltage sag amplitude. So, the best optimal value of the objective function found by GWO for voltage sag was 2.7945. When it comes to voltage swell, the values of Kp and Ki reveal that the PI tuning for mitigating was -8.15 and 67.813 when there was a voltage rise. Then, when compared to the PI, the PI-GWO has lower Kp and greater Ki values of -12.4826 and 349.7209, respectively. As a result, it has been demonstrated that in order to mitigate voltage swell and achieve a voltage rise of less than 6%, lower values of Kp and greater Ki in the voltage regulator are required to lessen the voltage swell amplitude. So, the best optimal value of the objective function found by GWO for voltage swell was 1.40119.

CHAPTER 5

CONCLUSION

5.1 Conclusion

This project aims to mitigate the voltage sag and swell by using PI-GWO during weak grid conditions. Before that, the system needs to be designed for a 5MW PV array using mathematical modelling. The PV array later will be used in a single-phase grid-connected system to identify the voltage sag and swell, in which the controller will be the GWO algorithm. Based on the designed PV array, the SunPower 210 W model was used as a reference model to run a simulation on a standard test. The I-V and P-V characteristic curves are obtained at the end of this simulation. The voltage sag and swell configurations was implemented inside the single-phase grid-connected PV system as it was used to analyse the effectiveness of PI-GWO to mitigate the voltage drop and voltage rise under different percentages of voltage sag and swell. As a conclusion, it is figured out that the PI-GWO method is more efficient to mitigate the voltage drop, and rise compared to the PI controller only. Although both of these controllers are capable to compensating for the voltage issue in the grid system, PI-GWO cope with both 10% and 20% of voltage sag and swell.

5.2 Future Recommendations

In this project, the proposed system objectives are to mitigate the voltage sag and swell during weak grid conditions by using the PI-GWO and to analyse the effectiveness of the proposed system under different percentages of voltage sag and swell. The results obtained can be improved in terms of voltage reduction. There are some suggestions for future work to improve the results of this project.

For instance, the controller can be replaced by a proportional-integral-derivative (PID) controller as it is able to restore the measured voltage to the desired voltage output with minimal delay and less noise or interruption by adjusting the gains of the controller

49

in a controlled manner. This dynamic behaviour of the system can also be tested in various scenarios, such as a three-phase grid-connected PV system or other power quality issues - lower power factor or high harmonic in the distribution system.

Apart from that, the project could use some external devices as part of the project simulation accompanied by the GWO algorithm to ensure more stability in voltage output during weak grid conditions. Lastly, the proposed system needs to be tested in more critical weak grid conditions in the future as a consequence of unsymmetrical faults.

REFERENCES

Cherati, S. M., Azli, N. A., Ayob, S. M., & Mortezaei, A. (2011). Design of a current mode PI controller for a single-phase PWM inverter. *2011 IEEE Applied Power Electronics Colloquium, IAPEC 2011*, *April*, 180–184. https://doi.org/10.1109/IAPEC.2011.5779864

Dhas, G. J. S., & Prakash, T. R. D. (2011). A novel approach for voltage sag mitigation using FACTS device interline dynamic voltage restorer. *ICECT 2011 - 2011 3rd International Conference on Electronics Computer Technology*, *4*, 37–41. https://doi.org/10.1109/ICECTECH.2011.5941852

El-Sayed, M. M., Abou El-Ela, A. A., & El-Sehiemy, R. A. (2017). Effect of photovoltaic system on power quality in electrical distribution networks. *2016 18th International Middle-East Power Systems Conference, MEPCON 2016 - Proceedings*, *October 2017*, 1005–1012. https://doi.org/10.1109/MEPCON.2016.7837019

Francis, D., & Thomas, T. (2014). Mitigation of voltage sag and swell using dynamic voltage restorer. *2014 Annual International Conference on Emerging Research Areas: Magnetics, Machines and Drives, AICERA/ICMMD 2014 - Proceedings*. https://doi.org/10.1109/AICERA.2014.6908218

Gopinath, B. (2016). *Mitigation of Voltage Sag and Swell by Ant Colony Optimization Technique using DPFC*. *1*(7), 44–48.

Guha, D., Roy, P. K., & Banerjee, S. (2016). Load frequency control of large scale power system using quasi-oppositional grey wolf optimization algorithm. *Engineering Science and Technology, an International Journal*, *19*(4), 1693–1713. https://doi.org/10.1016/j.jestch.2016.07.004

Iwata, H., & Okada, K. (2014). *Greenhouse gas emissions and the role of the Kyoto Protocol*. 325–342. https://doi.org/10.1007/s10018-012-0047-1

Jaalam, N., Ahmad, A. Z., Khalid, A. M. A., Abdullah, R., Saad, N. M., Ghani, S. A., & Muhammad, L. N. (2022). Low Voltage Ride through Enhancement Using Grey Wolf Optimizer to Reduce Overshoot Current in the Grid-Connected PV System. *Mathematical Problems in Engineering*, *2022*, 1–12. https://doi.org/10.1155/2022/3917775

Lee, D. M., Habetler, T. G., Harley, R. G., Rostron, J., & Keister, T. (2004). A voltage sag supporter utilizing a PWM-switched autotransformer. *PESC Record - IEEE Annual Power Electronics Specialists Conference*, *6*(2), 4244–4250. https://doi.org/10.1109/PESC.2004.1354751

Mehranfar, H., Baghramian, A., & Rafieinia, F. (2011). Mitigation of voltage swell by switched autotransformer with random hysteresis voltage control. *Asia-Pacific Power and Energy Engineering Conference, APPEEC*, 1–4. https://doi.org/10.1109/APPEEC.2011.5749002

Meloni, L. F. J., Rezek, Â. J. J., & Ribeiro, Ê. R. (2016). Small-signal modeling of a single-phase DVR for voltage sag mitigation. *Proceedings of International Conference on Harmonics and Quality of Power, ICHQP, 2016-Decem*, 55–59. https://doi.org/10.1109/ICHQP.2016.7783449

Mirjalili, S., Mirjalili, S. M., & Lewis, A. (2014). Grey Wolf Optimizer. *Advances in Engineering Software*, *69*, 46–61. https://doi.org/10.1016/j.advengsoft.2013.12.007

Premkumar, K., Kandasamy, P., Priya, M. V., Palanikumar, P., & Carter, S. B. R. (2019). Grey wolf Optimized PID Voltage and Power Factor Controlled AC to DC System. *International Journal of Innovative Technology and Exploring Engineering*, *9*(2), 5215–5220. https://doi.org/10.35940/ijitee.b7508.129219

Quirl, B. J., Johnson, B. K., & Hess, H. L. (2006). Mitigation of voltage sags with phase jump using a Dynamic Voltage Restorer. *2006 38th Annual North American Power Symposium, NAPS-2006 Proceedings*, 647–654. https://doi.org/10.1109/NAPS.2006.359640

Rauf, A. M., & Khadkikar, V. (2015). An Enhanced Voltage Sag Compensation Scheme for Dynamic Voltage Restorer. *IEEE Transactions on Industrial Electronics*, *62*(5), 2683–2692. https://doi.org/10.1109/TIE.2014.2362096

Salmi, T., Bouzguenda, M., Gastli, A., & Masmoudi, A. (2012). MATLAB/simulink based modelling of solar photovoltaic cell. *International Journal of Renewable Energy Research*, *2*(2), 213–218. https://doi.org/10.20508/ijrer.42248

Selvaraj, J., & Rahim, N. A. (2009). Multilevel Inverter For Grid-Connected PV System Employing Digital PI Controller. *IEEE Transactions on Industrial Electronics*, *56*(1), 149–158. https://doi.org/10.1109/TIE.2008.928116

Shah Alam, S., Omar, N. A., Bin Ahmad, M. S., Siddiquei, H. R., & Mohd. Nor, S. (2013). Renewable Energy in Malaysia: Strategies and Development. *Environmental Management and Sustainable Development*, *2*(1). https://doi.org/10.5296/emsd.v2i1.3197

Suja, K. R. (2021). Mitigation of power quality issues in smart grid using levy flight based moth flame optimization algorithm. *Journal of Ambient Intelligence and Humanized Computing*, *12*(10), 9209–9228. https://doi.org/10.1007/s12652-020-02626-3

Sule, A. H., Mokhtar, A. S., Bin Jamian, J. J., Sheikh, U. U., & Khidrani, A. (2020). Grey Wolf Optimizer Tuned PI Controller for Enhancing Output Parameters of Fixed Speed Wind Turbine. *2020 IEEE International Conference on Automatic Control and Intelligent Systems, I2CACIS 2020 - Proceedings, June*, 118–122. https://doi.org/10.1109/I2CACIS49202.2020.9140171
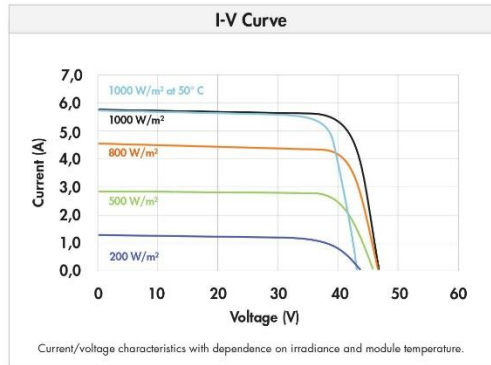
Figure 5.1   Reference PV model

APPENDIX B
GWO ALGORITHM MATLAB CODING

Main Function

```matlab
%_____%
%  Grey Wolf Optimizer (GWO) source codes version 1.0   %
%                                                        %
%  Developed in MATLAB R2011b(7.13)                      %
%                                                        %
%  Author and programmer: Seyedali Mirjalili            %
%                                                        %
%          e-Mail: ali.mirjalili@gmail.com              %
%                  seyedali.mirjalili@griffithuni.edu.au %
%                                                        %
%       Homepage: http://www.alimirjalili.com           %
%                                                        %
%   Main paper: S. Mirjalili, S. M. Mirjalili, A. Lewis %
%               Grey Wolf Optimizer, Advances in Engineering %
%               Software , in press,                    %
%               DOI: 10.1016/j.advengsoft.2013.12.007   %
%                                                        %
%_____%

% You can simply define your cost in a seperate file and load its
handle to fobj
% The initial parameters that you need are:
%_____
% fobj = @YourCostFunction
% dim = number of your variables
% Max_iteration = maximum number of generations
% SearchAgents_no = number of search agents
% lb=[lb1,lb2,...,lbn] where lbn is the lower bound of variable n
% ub=[ub1,ub2,...,ubn] where ubn is the upper bound of variable n
% If all the variables have equal lower bound you can just
% define lb and ub as two single number numbers

% To run GWO:
[Best_score,Best_pos,GWO_cg_curve]=GWO(SearchAgents_no,Max_iteration,l
b,ub,dim,fobj)
%_____

warning('off','all')
warning
clear all
clc

SearchAgents_no = 5; % Number of search agents
Max_iteration = 30; % Maximum numbef of iterations
dim = 2;
lb = [0 55];
ub = [150 5000];
fobj = @of;

[Best_score,Best_pos,GWO_cg_curve]=GWO(SearchAgents_no,Max_iteration,l
b,ub,dim,fobj);
```

```matlab
figure(1)

%Draw objective space

semilogy(GWO_cg_curve)

title('Objective space')
xlabel('Iteration');
ylabel('Best score obtained so far');

axis tight
grid on
box on

display(['The best solution obtained by GWO is : ',
num2str(Best_pos)]);
display(['The best optimal value of the objective funciton found by
GWO is : ', num2str(Best_score)]);
```

GWO Function

```matlab
% Grey Wolf Optimizer
function
[Alpha_score,Alpha_pos,Convergence_curve]=GWO(SearchAgents_no,Max_iter
,lb,ub,dim,fobj)

% initialize alpha, beta, and delta_pos
Alpha_pos=zeros(1,dim);
Alpha_score=inf; %change this to -inf for maximization problems

Beta_pos=zeros(1,dim);
Beta_score=inf; %change this to -inf for maximization problems

Delta_pos=zeros(1,dim);
Delta_score=inf; %change this to -inf for maximization problems

%Initialize the positions of search agents
x=initialization(SearchAgents_no,dim,ub,lb);

Convergence_curve=zeros(1,Max_iter);

l=0;% Loop counter
Interation=0;
Current_Position=0;
% Main loop
while l<Max_iter
    Interation = 1;
    for i=1:size(x,1)
        Current_Position = i
        % Return back the search agents that go beyond the boundaries
of the search space
        Flag4ub=x(i,:)>ub;
        Flag4lb=x(i,:)<lb;
        x(i,:)=(x(i,:).*(~(Flag4ub+Flag4lb)))+ub.*Flag4ub+lb.*Flag4lb;
```

```matlab
        % Calculate objective function for each search agent
        fitness=fobj(x(i,:));

        % Update Alpha, Beta, and Delta
        if fitness<Alpha_score
            Alpha_score=fitness; % Update alpha
            Alpha_pos=x(i,:);
        end

        if fitness>Alpha_score && fitness<Beta_score
            Beta_score=fitness; % Update beta
            Beta_pos=x(i,:);
        end

        if fitness>Alpha_score && fitness>Beta_score &&
fitness<Delta_score
            Delta_score=fitness; % Update delta
            Delta_pos=x(i,:);
        end
    end


    a=2-l*((2)/Max_iter); % a decreases linearly fron 2 to 0

    % Update the Position of search agents including omegas
    for i=1:size(x,1)
        for j=1:size(x,2)

            r1=rand(); % r1 is a random number in [0,1]
            r2=rand(); % r2 is a random number in [0,1]

            A1=2*a*r1-a; % Equation (3.3)
            C1=2*r2; % Equation (3.4)

            D_alpha=abs(C1*Alpha_pos(j)-x(i,j)); % Equation (3.5)-part
1
            X1=Alpha_pos(j)-A1*D_alpha; % Equation (3.6)-part 1

            r1=rand();
            r2=rand();

            A2=2*a*r1-a; % Equation (3.3)
            C2=2*r2; % Equation (3.4)

            D_beta=abs(C2*Beta_pos(j)-x(i,j)); % Equation (3.5)-part 2
            X2=Beta_pos(j)-A2*D_beta; % Equation (3.6)-part 2

            r1=rand();
            r2=rand();

            A3=2*a*r1-a; % Equation (3.3)
            C3=2*r2; % Equation (3.4)

            D_delta=abs(C3*Delta_pos(j)-x(i,j)); % Equation (3.5)-part
3
            X3=Delta_pos(j)-A3*D_delta; % Equation (3.5)-part 3
```

```
            x(i,j)=(X1+X2+X3)/3;% Equation (3.7)

        end
    end
    l=l+1;
    Convergence_curve(l)=Alpha_score;
end
```

Initialization Function

```
% This function initialize the first population of search agents
function Positions=initialization(SearchAgents_no,dim,ub,lb)

Boundary_no= size(ub,2); % numnber of boundaries

% If the boundaries of all variables are equal and user enter a signle
% number for both ub and lb
if Boundary_no==1
    Positions=rand(SearchAgents_no,dim).*(ub-lb)+lb;
end

% If each variable has a different lb and ub
if Boundary_no>1
    for i=1:dim
        ub_i=ub(i);
        lb_i=lb(i);
        Positions(:,i)=rand(SearchAgents_no,1).*(ub_i-lb_i)+lb_i;
    end
end
```

Objective Function

```
%cost function
function Cost = of( x )
kp=x(1);
ki=x(2);
options = simset('SrcWorkspace', 'current', 'DstWorkspace',
'current');
assignin('base','x',x);
sim('PI_GWO.slx',[0 0.5], options);
Cost=ITAE(length(ITAE));
end
```